At more rapid pacing rates, accumulation of ROS is anticipated, which would decrease I_{Na}. The CVs of the WT and mutant channel–transduced cultures are greater than that of nontransfected control cultures at slower pacing rates; at faster rates, the difference is diminished and no longer significant at a pacing cycle length of 180 ms (Figure 5B). The CVs of the WT-infected cultures are significantly increased by exposure to isoproterenol while that of the mutant-infected cultures are no more responsive than nontransfected control cultures (Figure 5C).

Discussion

Mutations in the Na channel, *SCN5A*,[10] or regulatory proteins such as *GPD1-L*[12] that reduce current have been associated with BrS and sudden infant death syndrome (SIDS). In both conditions, arrhythmias are more prevalent under conditions of various types of stress (oxidant stress, fever, ischemia, and Na channel blocking drugs). We describe an *SCN5A* mutation in a patient with BrS that produces both a chronic reduction in I_{Na} and absence of augmentation of the current by adrenergic stimulation. Interestingly, the reduction in the basal current produced by the R526H and S528A mutations compared with WT $Na_v1.5$ is more pronounced when fluoride is included in the patch pipette to inhibit protein phosphatase, consistent with increased basal phosphorylation of the WT channel. The elimination of a PKA site seems to be central to both the signaling and trafficking deficits. The disease-causing mutation, R526H, which is chemically and structurally conservative,[25,26] eliminates the basic priming residue in a consensus PKA phosphorylation recognition sequence. Replacement of the phosphorylation target residue, S528A, alters channel trafficking and regulation by PKA in a manner that is comparable to the disease-causing mutation and similar to previously described defects in PKA-mediated I_{Na} potentiation.[27] The mutations reduce channel expression at the membrane surface as assessed by biotinylation and immunocytochemistry

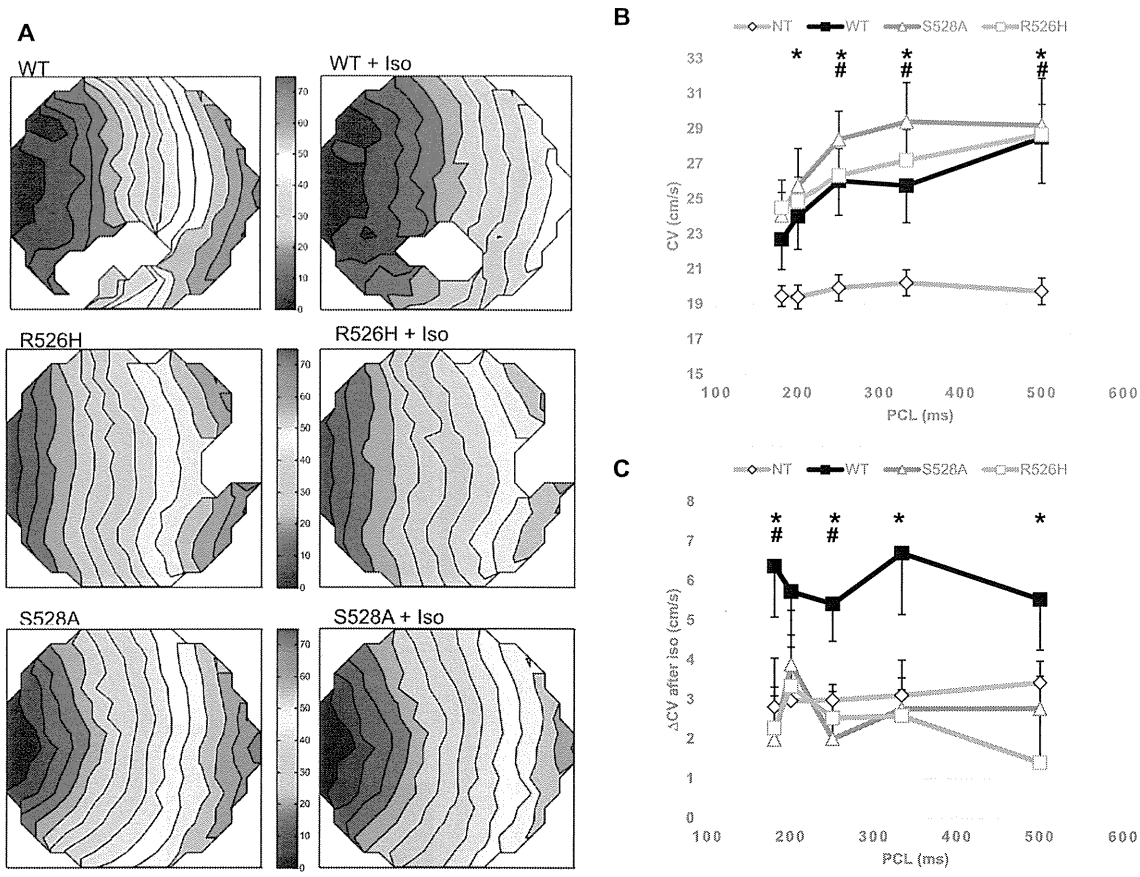

Figure 5. Optical mapping of Na channel variants. **A**, Representative isochronal maps from cultures of neonatal rat ventricular myocytes infected with the Na channel variants and stimulated at the left side of the culture. **B**, Plots of the average conduction velocity (CV)±SEM of wild-type (WT), R526H, and S528A transduced cultures and noninfected (NT) control cultures over a range of pacing cycle lengths (PCLs). CV is consistently faster in WT, R526H, and S528A $Na_v1.5$ infected cultures compared with the NT controls for the entire range of PCLs. *P<0.05, all vs NT; #P<0.01, all vs NT. **C**, Plots of the change in average CV±SEM of WT, R526H, and S528A transduced cultures and NT control cultures after application of 1 μmol/L isoproterenol. The change in CV of WT-transduced cultures is significantly larger than CV changes of NT cultures and mutant transduced cultures after isoproterenol application. *P<0.05, R526H vs WT; #P<0.05, S528A vs WT. The number of cultures studied at all PCLs in both the absence and presence of isoproterenol were NT (14), WT (13), S528A (5), and R526H (11).

studies (Figure 4) and are reflected in a lower expressed current density in HEK cells (Figure 3).

The reduction in I_{Na} is further complicated by the absence of a response of the channel to adrenergic stimulation. Neither the direct activation of adenylyl cyclase nor β-adrenergic stimulation with isoproterenol had a significant effect on current density or CV mediated by the mutant channel variants. These findings suggest a mechanism of stress-induced arrhythmias that may be due to changes of cellular redox balance with alterations in the ratio of NAD/NADH and consequent reduction in I_{Na}. Such metabolic stressors are typically accompanied by activation of the sympathetic nervous system that may partially offset the redox-induced reduction in I_{Na} and would dampen stress-induced ECG changes in BrS and alterations in CV. In such cases, arrhythmias would not be predicted to be induced by sympathetic activation but instead would be mitigated by an increase in sympathetic tone. This concept is consistent with the utility of isoproterenol in the treatment of arrhythmic storm in patients with BrS.[28–30]

There are several mechanisms by which metabolism has been proposed to alter the I_{Na}. Direct oxidation of the channel can alter channel conductance,[31,32] gating,[33,34] and trafficking.[35] Mutations associated with BrS have informed other mechanisms of metabolic regulation of Na channels. NADH is generated from NAD during glycolysis, and NAD must be regenerated for glycolysis to continue. *GPD1* reduces dihydroxyacetone phosphate to glycerol-3-phosphate, causing oxidation of NADH and regeneration of NAD with the electrons released from this reaction entering the electron transport chain. *GPD1-L* is highly homologous to *GPD1* and harbors mutations associated with BrS.[12] When mutant *GPD1-L* is coexpressed with $Na_v1.5$, I_{Na} is significantly reduced.[12–15] The BrS mutations have been proposed to reduce the enzymatic function of *GPD1-L* and would be expected to increase intracellular NADH levels. An increase in NADH possibly via activation of PKC,[13] enhancing phosphorylation of complex III resulting in an increase in ROS release,[14] reduces channel function. Alternatively, inactivating mutants of *GPD1-L* have been proposed to increase PKC phosphorylation of the Na channel in the III-IV linker, reducing current density.[15] Increased mitochondrial ROS release, elevated levels of NADH, and PKC activation have been implicated in I_{Na} downregulation in models of nonischemic cardiomyopathy and in CV slowing in diseased human ventricles.[36] Our work supports another mechanism of coupling of metabolism to channel function through altered PKA activation.[27] Increased NADH causes a reduction in current through WT and mutant R526H- and S528A-expressed channels. The absence of the PKA phosphorylation site in the mutant channels precludes current augmentation in the setting of sympathetic activation.

The mechanism of arrhythmias in this *SCN5A*-mediated BrS seems to involve a substrate that is characterized by decreased basal current expression as a result of altered mutant channel trafficking. Although it is difficult to infer general mechanisms from a single family, this disease-causing mutation produces the requisite basal reduction in I_{Na} compounded by defective current augmentation that generates the substrate for a potentially lethal arrhythmias. A trigger that further reduces I_{Na}, through any number of mechanisms such as alterations in glycolysis, ROS levels, or PKC activation, cannot be mitigated by PKA activation, leading to a further reduction in current. The absence of a PKA-mediated reversal of NADH-induced current reduction (Figure 3) is consistent with the lack of effect on conduction in infected NRVMs. The reduction of I_{Na} could alter either regional dispersion of repolarization or conduction in the heart; one or both may contribute to the genesis of the potentially lethal ventricular arrhythmias in patients harboring this mutation.

Acknowledgments

We thank Deborah DiSilvestre, Victoria Halperin Kuhns, and Dr Yan Li Tian for technical support.

Sources of Funding

The work was supported by R01 HL 50411 (G.F. Tomaselli) and a Mid-Atlantic Affiliate AHA fellowship (G. Kostecki).

Disclosures

None.

References

1. Antzelevitch C, Brugada P, Borggrefe M, Brugada J, Brugada R, Corrado D, et al. Brugada syndrome: report of the second consensus conference: endorsed by the Heart Rhythm Society and the European Heart Rhythm Association. *Circulation*. 2005;111:659–670.
2. Martini B, Nava A, Thiene G, Buja GF, Canciani B, Scognamiglio R, et al. Ventricular fibrillation without apparent heart disease: description of six cases. *Am Heart J*. 1989;118:1203–1209.
3. Haïssaguerre M, Derval N, Sacher F, Jesel L, Deisenhofer I, de Roy L, et al. Sudden cardiac arrest associated with early repolarization. *N Engl J Med*. 2008;358:2016–2023.
4. Hoogendijk MG, Opthof T, Postema PG, Wilde AA, de Bakker JM, Coronel R. The Brugada ECG pattern: a marker of channelopathy, structural heart disease, or neither? Toward a unifying mechanism of the Brugada syndrome. *Circ Arrhythm Electrophysiol*. 2010;3:283–290.
5. Patel SS, Anees S, Anees SS, Ferrick KJ. Prevalence of a Brugada pattern electrocardiogram in an urban population in the United States. *Pacing Clin Electrophysiol*. 2009;32:704–708.
6. Sinner MF, Pfeufer A, Perz S, Schulze-Bahr E, Mönnig G, Eckardt L, et al. Spontaneous Brugada electrocardiogram patterns are rare in the German general population: results from the KORA study. *Europace*. 2009;11:1338–1344.
7. Sidik NP, Quay CN, Loh FC, Chen LY. Prevalence of Brugada sign and syndrome in patients presenting with arrhythmic symptoms at a Heart Rhythm Clinic in Singapore. *Europace*. 2009;11:650–656.
8. Nademanee K, Veerakul G, Nimmannit S, Chaowakul V, Bhuripanyo K, Likittanasombat K, et al. Arrhythmogenic marker for the sudden unexplained death syndrome in Thai men. *Circulation*. 1997;96:2595–2600.
9. Priori SG, Wilde AA, Horie M, Cho Y, Behr ER, Berul C, et al; Document Reviewers; Heart Rhythm Society; European Heart Rhythm Association; Asia Pacific Heart Rhythm Society. Executive summary: HRS/EHRA/APHRS expert consensus statement on the diagnosis and management of patients with inherited primary arrhythmia syndromes. *Europace*. 2013;15:1389–1406.
10. Chen Q, Kirsch GE, Zhang D, Brugada R, Brugada J, Brugada P, et al. Genetic basis and molecular mechanism for idiopathic ventricular fibrillation. *Nature*. 1998;392:293–296.
11. Miura D, Nakamura K, Ohe T. Update on genetic analysis in Brugada syndrome. *Heart Rhythm*. 2008;5:1495–1496.
12. London B, Michalec M, Mehdi H, Zhu X, Kerchner L, Sanyal S, et al. Mutation in glycerol-3-phosphate dehydrogenase 1 like gene (GPD1-L) decreases cardiac Na+ current and causes inherited arrhythmias. *Circulation*. 2007;116:2260–2268.
13. Liu M, Sanyal S, Gao G, Gurung IS, Zhu X, Gaconnet G, et al. Cardiac Na+ current regulation by pyridine nucleotides. *Circ Res*. 2009;105:737–745.
14. Liu M, Liu H, Dudley SC Jr. Reactive oxygen species originating from mitochondria regulate the cardiac sodium channel. *Circ Res*. 2010;107:967–974.
15. Valdivia CR, Ueda K, Ackerman MJ, Makielski JC. GPD1L links redox state to cardiac excitability by PKC-dependent phosphorylation of the sodium channel SCN5A. *Am J Physiol Heart Circ Physiol*. 2009;297:H1446–H1452.

16. Chahine M. Cardiac metabolic state and Brugada syndrome: a link revealed. *Circ Res*. 2009;105:721–723.
17. Fleming J, Ginn SL, Weinberger RP, Trahair TN, Smythe JA, Alexander IE. Adeno-associated virus and lentivirus vectors mediate efficient and sustained transduction of cultured mouse and human dorsal root ganglia sensory neurons. *Hum Gene Ther*. 2001;12:77–86.
18. Kizana E, Chang CY, Cingolani E, Ramirez-Correa GA, Sekar RB, Abraham MR, et al. Gene transfer of connexin43 mutants attenuates coupling in cardiomyocytes: novel basis for modulation of cardiac conduction by gene therapy. *Circ Res*. 2007;100:1597–1604.
19. Sekar RB, Kizana E, Cho HC, Molitoris JM, Hesketh GG, Eaton BP, et al. IK1 heterogeneity affects genesis and stability of spiral waves in cardiac myocyte monolayers. *Circ Res*. 2009;104:355–364.
20. Biswas S, DiSilvestre D, Tian Y, Halperin VL, Tomaselli GF. Calcium-mediated dual-mode regulation of cardiac sodium channel gating. *Circ Res*. 2009;104:870–878.
21. Bursac N, Parker KK, Iravanian S, Tung L. Cardiomyocyte cultures with controlled macroscopic anisotropy: a model for functional electrophysiological studies of cardiac muscle. *Circ Res*. 2002;91:e45–e54.
22. Sekar RB, Kizana E, Smith RR, Barth AS, Zhang Y, Marbán E, et al. Lentiviral vector-mediated expression of GFP or Kir2.1 alters the electrophysiology of neonatal rat ventricular myocytes without inducing cytotoxicity. *Am J Physiol Heart Circ Physiol*. 2007;293:H2757–H2770.
23. Aiba T, Hesketh GG, Liu T, Carlisle R, Villa-Abrille MC, O'Rourke B, et al. Na+ channel regulation by Ca2+/calmodulin and Ca2+/calmodulin-dependent protein kinase II in guinea-pig ventricular myocytes. *Cardiovasc Res*. 2010;85:454–463.
24. Exome variant server. Available at: http://evs.gs.washington.edu/EVS/. Accessed November 11, 2013.
25. Grantham R. Amino acid difference formula to help explain protein evolution. *Science*. 1974;185:862–864.
26. Adzhubei IA, Schmidt S, Peshkin L, Ramensky VE, Gerasimova A, Bork P, et al. A method and server for predicting damaging missense mutations. *Nat Methods*. 2010;7:248–249.
27. Zhou J, Shin HG, Yi J, Shen W, Williams CP, Murray KT. Phosphorylation and putative ER retention signals are required for protein kinase A-mediated potentiation of cardiac sodium current. *Circ Res*. 2002;91:540–546.
28. Miyazaki T, Mitamura H, Miyoshi S, Soejima K, Aizawa Y, Ogawa S. Autonomic and antiarrhythmic drug modulation of ST segment elevation in patients with Brugada syndrome. *J Am Coll Cardiol*. 1996;27:1061–1070.
29. Tanaka H, Kinoshita O, Uchikawa S, Kasai H, Nakamura M, Izawa A, et al. Successful prevention of recurrent ventricular fibrillation by intravenous isoproterenol in a patient with Brugada syndrome. *Pacing Clin Electrophysiol*. 2001;24(8, Part 1):1293–1294.
30. Maury P, Couderc P, Delay M, Boveda S, Brugada J. Electrical storm in Brugada syndrome successfully treated using isoprenaline. *Europace*. 2004;6:130–133.
31. Spalding BC. Properties of toxin-resistant sodium channels produced by chemical modification in frog skeletal muscle. *J Physiol*. 1980;305:485–500.
32. Sigworth FJ, Spalding BC. Chemical modification reduces the conductance of sodium channels in nerve. *Nature*. 1980;283:293–295.
33. Ward CA, Giles WR. Ionic mechanism of the effects of hydrogen peroxide in rat ventricular myocytes. *J Physiol*. 1997;500(Part 3):631–642.
34. Song Y, Shryock JC, Wagner S, Maier LS, Belardinelli L. Blocking late sodium current reduces hydrogen peroxide-induced arrhythmogenic activity and contractile dysfunction. *J Pharmacol Exp Ther*. 2006;318:214–222.
35. Hallaq H, Wang DW, Kunic JD, George AL Jr, Wells KS, Murray KT. Activation of protein kinase C alters the intracellular distribution and mobility of cardiac Na+ channels. *Am J Physiol Heart Circ Physiol*. 2012;302:H782–H789.
36. Liu M, Gu L, Sulkin MS, Liu H, Jeong EM, Greener I, et al. Mitochondrial dysfunction causing cardiac sodium channel downregulation in cardiomyopathy. *J Mol Cell Cardiol*. 2013;54:25–34.

CLINICAL PERSPECTIVE

Brugada syndrome is an inherited cardiac arrhythmia characterized by coved-type ST-segment elevation in the right precordial (V_1 and V_2) leads of the ECG and an increased risk of sudden cardiac death. In some cases, the cause is a mutation in *SCN5A*, the gene encoding the α-subunit of cardiac sodium channels, typically resulting in a loss of function. The genetic and cellular mechanisms of Brugada syndrome have provided general insights into the links between metabolism, ion channel function, and cardiac arrhythmias. Oxidant stress, as may occur with fever, ischemia, or even an increase in heart rate, can produce a potentially arrhythmogenic decrease in the sodium current (I_{Na}). We have described a mutation in a consensus protein kinase A phosphorylation site in a patient with Brugada syndrome that does not respond to sympathetic stimulation. Wild-type and Brugada syndrome mutant I_{Na} are reduced by oxidant stress and subsequent protein kinase A stimulation mitigates the reduction of the wild-type I_{Na} but not the current through mutant channels. This disease-causing mutation may have relevance to more general mechanisms of arrhythmias involving I_{Na}. A trigger that reduces I_{Na}, through any number of mechanisms that cannot be mitigated by protein kinase A activation, could produce a reduction in I_{Na} with an increased risk of cardiac arrhythmias.

Advance Publication by-J-STAGE

Circulation Journal
Official Journal of the Japanese Circulation Society
http://www.j-circ.or.jp

A Novel HCN4 Mutation, G1097W, Is Associated With Atrioventricular Block

Jun Zhou, PhD; Wei-Guang Ding, MD, PhD; Takeru Makiyama, MD, PhD; Akashi Miyamoto, MD, PhD; Yuichi Matsumoto, MD, PhD; Hiromi Kimura, MD; Yasuhiro Tarutani, MD, PhD; Jin Zhao, BSc; Jie Wu, PhD; Wei-Jin Zang, PhD; Hiroshi Matsuura, PhD; Minoru Horie, MD, PhD

Background: Loss-of-function mutations in the HCN4 gene have been shown to be associated with sinus dysfunction, but there are no reports on HCN4-mediated atrioventricular (AV) block. A novel missense HCN4 mutation G1097W was identified in a 69 year-old Japanese male with AV block, and we characterized the functional consequences of I_f-like channels reconstituted with the heterozygous HCN4 mutation.

Methods and Results: Wild-type (WT) HCN4 or/and HCN4-G1097W were expressed in a heterologous cell expression system. A functional assay using a whole-cell patch-clamp demonstrated that the mutant I_f-like currents were activated at more negative voltages compared to WT currents, while they retained the sensitivity to changes in intracellular cyclic adenosine monophosphate (cAMP) levels. Co-expression of G1097W with WT channels showed dominant-negative effects, including a reduction in peak currents and a negative voltage shifting on reconstituted currents.

Conclusions: The HCN4-G1097W mutant channels displayed a loss-of-function type modulation on cardiac I_f channels and thus could predispose them to AV nodal dysfunction. These data provide a novel insight into the genetic basis for the AV block.

Key Words: Atrioventricular (AV) block; I_f; Novel HCN4 mutation; Patch-clamp

The automaticity of heart rhythm is determined by a concerted function of various ion channels, including at least 4 different types of cation channels:[1–4] T- and L-type Ca^{2+} channels, K^+ channels, and the I_f channels that carries both K^+ and Na^+ ions under physiological conditions (relative permeability ratio: P_{Na}/P_K=0.2–0.4),[5] thereby producing a reversal potential of approximately –25 mV. I_f channels flow in an inward depolarizing current in pacemaker cells after the channels are repolarized by the activation of K^+ channels and they drive the cell membrane potential up to the threshold of Ca^{2+} channel activation. The activation of I_f channels generates the "pacemaker potential" and determines the rate of automaticity in nodal cells. I_f channel currents are regulated by intracellular cyclic adenosine monophosphate (cAMP) levels. In addition to hyperpolarization, an increase in cAMP accelerates the pacemaker potential rise by shifting the voltage dependence of I_f channels to a more positive potential.[3] This phenomenon explains the positive chronotropic effect of β-adrenergic receptor agonists.[6]

Genes encoding α-subunits of I_f channels have 4 members, the hyperpolarization-activated cyclic nucleotide-gated channels 1–4 (termed HCN1-HCN4).[3] HCN1, -2, and -4 are expressed in the heart and brain, and all have 6 transmembrane helices (S1–S6) and a cyclic nucleotide binding domain (cNBD) in the middle of the C-terminus.[3] Similar to other members of voltage-gated cation channels, the 4 subunits of the HCN channels most likely form a tetramer. Compared to other HCN isoforms, HCN4 is known to be more abundant in the heart.[7,8] HCN4 mutations are reported to cause familial sick sinus syndrome[9–11] and sporadic cases of sinus nodal dysfunction;[12] however, their relationship with atrioventricular (AV) block remains unknown. We recently identified a novel HCN4 mutation (G1097W) in a Japanese patient with AV block. The functional characterization of reconstituted I_f channels shows that the HCN4 mutation could predispose to AV nodal dysfunction, which might provide an important insight into the genetic basis for the AV block.

Received August 12, 2013; revised manuscript received November 29, 2013; accepted December 15, 2013; released online January 31, 2014 Time for primary review: 17 days

Department of Pharmacology, Medical School of Xi'an Jiaotong University, Xi'an (J. Zhou, J. Zhao, J.W., W.-J.Z.), China; Department of Physiology (W.-G.D., H.M.), Department of Cardiovascular and Respiratory Medicine (J. Zhou, A.M., Y.M., H.K., Y.T., M.H.), Shiga University of Medical Science, Otsu; and Department of Cardiovascular Medicine, Kyoto University Graduate School of Medicine, Kyoto (T.M.), Japan

Mailing address: Minoru Horie, MD, PhD, Department of Cardiovascular and Respiratory Medicine, Shiga University of Medical Science, Seta-Tsukinowa, Otsu 520-2192, Japan. E-mail: horie@belle.shiga-med.ac.jp or Jie Wu, PhD, Department of Pharmacology, Medical School of Xi'an Jiaotong University, Xi'an, Shaanxi 710061, China E-mail: wujie@mail.xjtu.edu.cn

ISSN-1346-9843 doi:10.1253/circj.CJ-13-0996

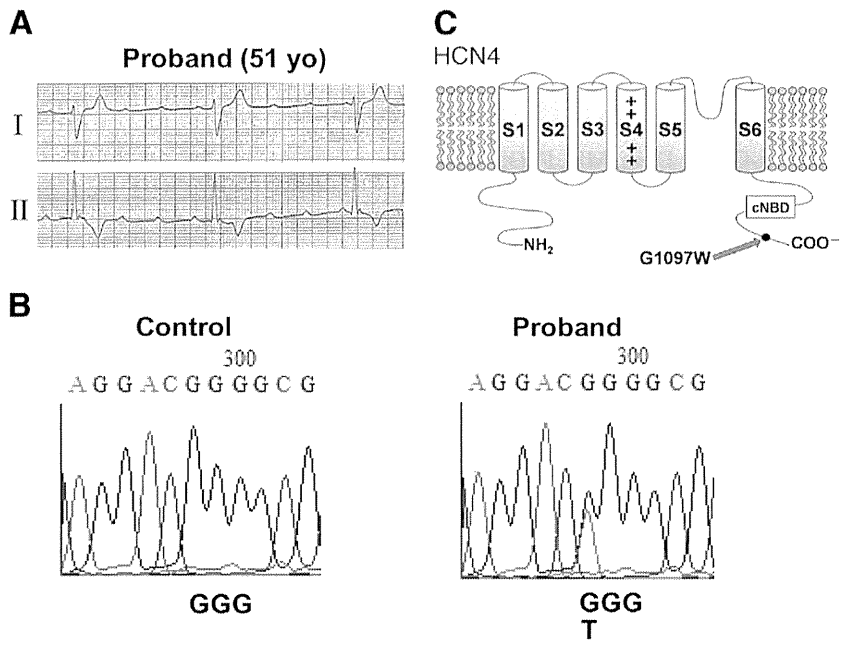

Figure 1. Clinical characterization and molecular discovery of HCN4-G1097W (a novel HCN4 mutation). (A) The patient's electrocardiograms (ECGs) indicating a complete AV block. (B) DNA sequence analyses demonstrate the location of the heterozygous mutation HCN4-G1097W (3289G>T). (C) Schematic topology of HCN4 channels. The location of the detected mutation is shown by the arrow.

Methods

Genetic Testing

After obtaining appropriate approval from the institution review board and written informed consent from the patient, genomic DNA was isolated from peripheral blood lymphocytes and screened for candidate genes by using denaturing high performance liquid chromatography (DHPLC: WAVE Model 3500, Transgenomic Inc, Omaha, NE, USA). We screened for SCN5A and HCN4 mutations in patients from 38 families with sick sinus syndrome or AV block. Abnormal conformers were amplified by using polymerase chain reaction (PCR), and sequencing was performed on an ABI PRISM 3100 DNA sequencer (Applied Biosystems, Foster City, CA, USA).

Cell Preparation, Site-Directed Mutagenesis, and Transfection

Chinese hamster ovary (CHO) cells were cultured in Dulbecco's Modified Eagle's Medium (DMEM)/F-12 supplemented with 2 mmol/L L-glutamine, 10% fetal calf serum (FCS), 100 U/ml penicillin, and 100 μg/ml streptomycin sulfate in an atmosphere of 95% air and 5% CO_2 at 37°C. Cells were passaged twice weekly by harvesting with trypsin-EDTA, and a part of the treated cells were seeded onto glass coverslips (5×3 mm^2) for transfection.

The mammalian expression vector, pcDNA3.0, containing HCN4 cDNA (provided by Dr Takano M, Kurume University, Japan) was used for the expression of all constructs in this study. PCR-based, site-directed mutagenesis was applied to introduce the HCN4-G1097W mutation into HCN4 cDNA by using a Quikchange Mutagenesis Kit (Stratagene, La Jolla, CA, USA). All PCR products were fully sequenced to ensure the fidelity of the PCR reactions. Wild-type (WT) HCN4 or/and G1097W cDNAs were transiently transfected into CHO cells together with green fluorescent protein (GFP) cDNA (1.5 μg HCN4-WT or -G1097W+0.5 μg GFP) by using Lipofectamine (Invitrogen Life Technologies, Carlsbad, CA, USA), according to the manufacturer's instructions.

Electrophysiological Recordings and Data Analysis

After a 48-h transfection, cells attached to glass coverslips were transferred to a recording chamber (0.5 ml) mounted on the stage of an inverted microscope (ECLIPSE TE2000-U; Nikon, Tokyo, Japan). The chamber was maintained at 25°C and was perfused continuously at a rate of 1–2 ml/min with Tyrode's solution. Patch-clamp experiments were conducted as described previously.[13] Whole-cell membrane currents were recorded with an EPC-8 patch-clamp amplifier (HEKA, Lambrecht, Germany). Current data were low-pass filtered at 1 kHz, acquired at 5 kHz through an LIH-1600 analogue-to-digital converter (HEKA), and stored on a hard disc drive, by using Pulse/Pulse Fit software (HEKA). Patch pipettes were fabricated from glass capillaries using a horizontal puller (P-97; Sutter Instruments Co, Novato, CA, USA). Patch electrodes had a resistance of 3–4MΩ when filled with the pipette solution containing (in mmol/L) 70 potassium aspartate, 40 KCl, 10 KH_2PO_4, 1 $MgSO_4$, 3 Na_2-ATP (Sigma Chemical Co, St. Louis, MO, USA), 0.1 Li_2-GTP (Roche Diagnostics GmbH, Mannheim, Germany), 5 EGTA and 5 HEPES (pH adjusted to 7.2 with KOH). Tyrode's solution contained (in mmol/L) 140 NaCl, 5.4 KCl, 1.8 $CaCl_2$, 0.5 $MgCl_2$,

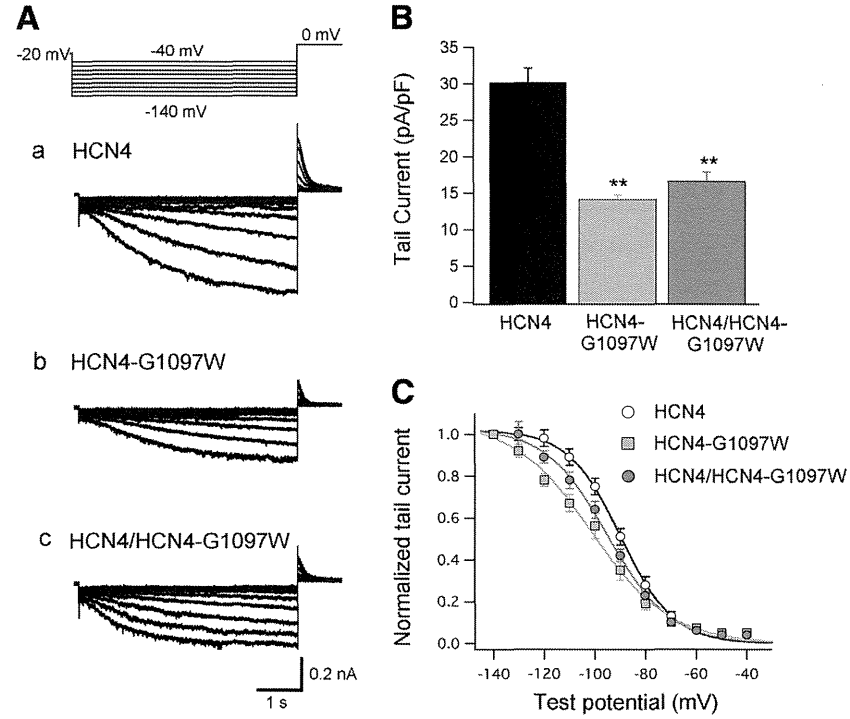

Figure 2. Functional characterization of HCN4-G1097W (a novel HCN4 mutation) channels in CHO cells. Representative current traces of HCN4-WT (**A-a**), HCN4-G1097W (**A-b**), and HCN4-WT/HCN4-G1097W (**A-c**) channels elicited by 5 s hyperpolarizing voltage steps between –40 mV and –120 mV from a holding potential of –20 mV. (**B**) Average peak tail current density of HCN4-WT, HCN4-G1097W, and HCN4-WT/G1097W at –120 mV (**P<0.01 vs. HCN4-WT). (**C**) Normalized tail currents are shown as a function of test potentials from 5 s test pulses. Each data set was fitted by the Boltzmann equation. Therefore, G1097W and HCN4-WT/HCN4-G1097W produced a negative shift of $V_{1/2}$ by 12 and 8 mV (P<0.01 and P<0.05 vs. HCN4-WT), respectively.

0.33 NaH_2PO_4, 5.5 glucose and 5.0 HEPES (pH was adjusted to 7.4 with NaOH). The cell was clamped at –20 mV and hyperpolarized to potentials from –40 mV to –120 mV for 5 s. Tail currents were observed at 0 mV and expressed as densities (pA/pF) to control for cell size variability. The voltage dependence of activation was fitted to the Boltzmann equation: relative tail currents=1/(1+exp ((V_m–$V_{1/2}$)/slope factor)), where V_m indicates test potentials and $V_{1/2}$ is the half activating potential. The deactivation kinetics of I_f was determined by fitting a single exponential function to the tail current trace at –120 mV.

Statistical Analysis

All data are expressed as mean±standard error of the mean (SEM), with the number of experiments in parentheses. Statistical comparisons were analyzed using a Student's unpaired t test and one-way analysis of variance (ANOVA) with Newman-Keuls post-hoc test. A P<0.05 was considered statistically significant.

Results

Clinical Investigation and Genetic Analysis

The patient was a 69-year-old male who underwent DDD pacemaker implantation (PMI) at the age of 51 years because of recurrent syncope. His electrocardiograph (ECG) before the operation showed a complete AV block with wide QRS but not sinus nodal dysfunction. The atrial rate was 132 beats per minute (bpm) and the ventricular rate was 33 bpm (**Figure 1A**). The high atrial rate might be compensation that resulted from an enhancement in sympathetic tone of the heart because the AV block leads to a slower ventricular rate (33 bpm) that reduces cardiac output and might cause ischemia. Genetic analysis identified a novel heterozygote missense mutation, HCN4-G1097W (3289G>T). **Figure 1B** shows the results of subsequent sequencing and **Figure 1C** illustrates the topology of HCN4 and the mutant location in the C-terminus, which was downstream to the cyclic nucleotide-binding domain (cNBD). Importantly, the mutation was absent in 110 Japanese control individuals (220 chromosomes).

Functional Analyses of HCN4-G1097W Channels

In order to analyze the functional characteristics of the HCN4-G1097W mutant channel, the whole-cell configuration of the patch-clamp technique was used. Upon hyperpolarizing membrane potentials (–40 mV to –140 mV for 5 s), cells transfected with WT, G1097W or WT+G1097W displayed slowly activating inward currents with typical I_f features,[6,7] as well as outward tail currents after returning to 0 mV (**Figures 2A-a–c**). As shown in **Figure 2B**, the tail current densities after a –140 mV repolarization pulse were 30.2±1.9 pA/pF (n=26) in

Table. Gating Kinetics of HCN4-G1097W Channels

	$V_{1/2}$ (mV)	Slope factor (mV)	Plus cAMP		τ of deactivation (ms)
			$V_{1/2}$ (mV)	Slope factor (mV)	
HCN4-WT	−86.6±1.7 (n=20)	8.9±0.3 (n=20)	−78.0±1.6 (n=12)	9.0±0.6 (n=12)	196.9±8.4 (n=22)
HCN4-G1097W	−98.6±3.1** (n=18)	12.4±1.2 (n=18)	−88.7±2.3 (n=9)	12.6±1.6 (n=9)	154.6±9.2** (n=18)
HCN4/HCN4-G1097W	−94.2±2.2* (n=19)	11.1±0.7 (n=19)	ND	ND	159.1±14.4* (n=13)

*P<0.05, **P<0.01 vs. WT.
cAMP, cyclic adenosine monophosphate; HCN4-G1097W, a novel HCN4 mutation; ND, not detected; $V_{1/2}$, half activating potential; WT, wild type.

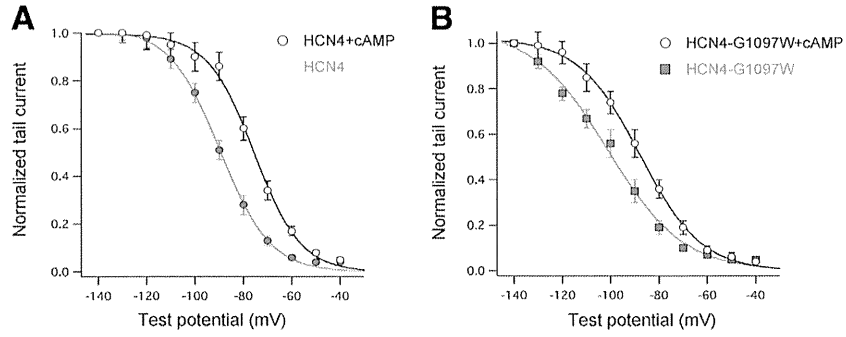

Figure 3. Effects of cyclic adenosine monophosphate (cAMP) on tail currents of HCN4-WT and HCN4-G1097W (a novel HCN4 mutation) channels in CHO cells. Current-voltage (*I-V*) relations for tail currents of HCN4-WT (A) and HCN4-G1097W (B) in the presence (open circles) or absence (closed circles) of 1 mmol/L 8-Br-cAMP. The tail currents were recorded at 0 mV after hyperpolarization to potentials from −40 mV to −140 mV for 5 s. HCN4+cAMP and HCN4-G1097W+cAMP produced a positive shift of $V_{1/2}$ by 9 and 10 mV (P<0.01 and P<0.05 vs. HCN4 and HCN4-G1097W), respectively.

HCN4-WT, 14.1±0.6 pA/pF in HCN4-G1097W (P<0.01 vs. WT, n=26), and 16.6±1.3 pA/pF (P<0.01 vs. WT, n=25) in WT+HCN4-G1097W. The current densities in both HCN4-G1097W and WT+HCN4-G1097W channels were similar and significantly smaller than that of WT. Moreover, the deactivation time constants were significantly faster in mutant channels compared to that of WT channels (Table). Open probabilities of WT, mutant, and WT/mutant channels were taken from instantaneous peak outward tail currents by normalizing with those recorded after −140 mV hyperpolarization, and were plotted as a function of test potential (Figure 2C). All relations were well described by the Boltzmann function. Compared to WT, both mutant and WT/mutant channels showed significantly negative shifts (approximately −12 mV and −8 mV, respectively) in half-activation potentials ($V_{1/2}$) and had larger slope factors (Table). The results suggested that the HCN4-G1097W mutation had a suppressive effect on WT-HCN4 channels.

To investigate the effects of cAMP on HCN4-G1097W channel currents, a cAMP analog, 8-Br-cAMP (Sigma Chemical Co), was intracellularly loaded through a recording pipette. Figure 3 and Table show that the midpoints ($V_{1/2}$) of activation of HCN4-WT (Figure 3A) and HCN4-G1097W (Figure 3B) currents were shifted approximately 9 mV and 10 mV towards the depolarization direction with an intracellular dialysis of 1 mmol/L 8-Br-cAMP for 5–7 min, respectively. There was no significant difference between the shifts of the 2 current activations in the presence of cAMP.

Discussion

In the present study, we identified a novel missense HCN4 mutation, G1097W, in a Japanese male patient with AV nodal dysfunction. Functional analyses showed that HCN4-G1097W caused a loss-of-function suppression on I_f channels, possibly leading to AV nodal dysfunction. To the best of our knowledge, this is the first report on the HCN4 mutation related to AV block but not sinus nodal dysfunction.[9–11]

HCN4 Mutations and Sinus Nodal Dysfunction

Four HCN4 mutations have been reported to be associated with sinus bradycardia, intermittent episodes of atrial fibrillation (P573X),[12] severe bradycardia, QT prolongation, torsade de pointes (D553N),[9] asymptomatic sinus bradycardia (S672R),[10] or sinus bradycardia (G480R).[11] However, AV block was not a complication in any of these reports. Although grade II or greater AV block has been recognized in ~70% patients with sick sinus syndrome,[14–17] there is no case of binodal dysfunction associated with HCN4 mutations.

Previous functional assays on HCN4 mutant channels have revealed various biophysical outcomes associated with I_f: (1) the negative shift of the activation gate (P573X, G480R, and S672R);[10–12] (2) reduction in current densities (D553N and G480R);[9,11] (3) slower activation (G480R);[9] (4) faster deactivation (S672R);[10] and (5) reduced sensitivity to intracellular cAMP (P573X).[12] These results implicate a potential association of I_f current decrease during diastolic depolarization with

a slowing of the sinus rate. These 4 HCN4 mutations provide evidence that HCN4 channels are essential for proper sinus pacemaker activity in humans.

Unique Properties of the HCN4-G1097W Mutation

Unlike previous reports, the carrier of HCN4-G1097W in this study suffered from AV block but not sick sinus syndrome. His clinical features were similar to those of familial progressive heart block or cardiac conduction disturbance (PCCD: Lenegre disease). It remains unknown why the patient was exclusively affected by AV block. In this regard, Habuchi et al[18] and Munk et al[19] demonstrated that I_f is expressed in ~90% of isolated rabbit AV nodal cells, suggesting that I_f does play an important role in generating AV junctional pacemaking. More recently, Dobrzynski et al[20] used histological and immunohistochemical techniques to show that the role of I_f might be even more important in the posterior extension from the AV node than in the sinus node. In addition, Marger et al indicated that HCN4 channels are important for basal excitability of mouse AV node cells.[2] All these implicate that a HCN4 mutation might lead to AV nodal dysfunction.

A biophysical survey of the HCN4-G1097W mutation (Figures 2,3) showed that it caused a loss-of-function effect on the I_f current by shifting the activation gate to a more hyperpolarizing state and reducing the current density. In heterozygous conditions, the mutation also significantly attenuated I_f channel functions (Figure 2). Therefore, HCN4-G1097W most likely predisposes to the AV block, leading to a slow ventricular rate (33 bpm) in our patient. The slow ventricular rate reduces cardiac output and stimulates the sympathetic nervous system reflexly, causing the higher activity of the SA node (even a normal SA function) because of the higher density of sympathetic innervation.[21–23] That might (at least partially) be the reason why our patient first presented with AV block but not SA dysfunction. Similar to progressive cardiac conduction defect cases, our patient showed AV conduction disturbances at an age over 50 years. Therefore, other genetic or environmental factors might predispose the patient to the apparent pathological conditions.[24] Further studies involving more HCN4 mutation cases are needed to elucidate the underlying mechanisms.

In the present study, HCN4-G1097W, which is located close to the cNBD in the C-terminus (Figure 1C), does not change the response of I_f to intracellular cAMP, suggesting that the mutation has no effect on the combination of cAMP with cNBD or the activation of I_f by cAMP.[25]

Acknowledgments

We are grateful to Ms Arisa Ikeda and Ms Yoko Mitsuyama for their excellent technical assistance. This work was supported by Grants-in-Aid in Scientific Research from the Ministry of Education, Culture, Sports, Science, Technology and the Ministry of Health, Labor, and Welfare of Japan, and the Uehara Memorial Foundation (M.H.), and by the National Natural Science Foundation of China (No. 81170176 to J.Z.; No. 81273501 to J.W. and W.G.D.), the Scientific Research Foundation for Returned Overseas Chinese Scholars of State Education Ministry grant (20 returned fund 08 to J.Z.) and by the Major International (Regional) Joint Research Project of the National Natural Science Foundation of China (No. 81120108002 to W.J.Z.).

Disclosures

Conflicts of Interest: None.

References

1. Irisawa H, Brown HF, Giles W. Cardiac pacemaking in the sinoatrial node. *Physiol Rev* 1993; **73:** 197–227.
2. Marger L, Mesirca P, Alig J, Torrente A, Dubel S, Engeland B, et al. Functional roles of Ca(v)1.3, Ca(v)3.1 and HCN channels in automaticity of mouse atrioventricular cells: Insights into the atrioventricular pacemaker mechanism. *Channels (Austin)* 2011; **5:** 251–261.
3. Biel M, Schneider A, Wahl C. Cardiac HCN channels: Structure, function, and modulation. *Trends Cardiovasc Med* 2002; **12:** 206–212.
4. Fujii H, Ikeuchi Y, Kurata Y, Ikeda N, Bahrudin U, Li P, et al. Electrophysiological properties of prion-positive cardiac progenitors derived from murine embryonic stem cells. *Circ J* 2012; **76:** 2875–2883.
5. Pape HC. Queer current and pacemaker: The hyperpolarization-activated cation current in neurons. *Annu Rev Physiol* 1996; **58:** 299–327.
6. DiFrancesco D, Tortora P. Direct activation of cardiac pacemaker channels by intracellular cyclic AMP. *Nature* 1991; **351:** 145–147.
7. Ludwig A, Zong X, Stieber J, Hullin R, Hofmann F, Biel M. Two pacemaker channels from human heart with profoundly different activation kinetics. *EMBO J* 1999; **18:** 2323–2329.
8. Seifert R, Scholten A, Gauss R, Mincheva A, Lichter P, Kaupp UB. Molecular characterization of a slowly gating human hyperpolarization-activated channel predominantly expressed in thalamus, heart, and testis. *Proc Natl Acad Sci USA* 1999; **96:** 9391–9396.
9. Ueda K, Nakamura K, Hayashi T, Inagaki N, Takahashi M, Arimura T, et al. Functional characterization of a trafficking-defective HCN4 mutation, D553N, associated with cardiac arrhythmia. *J Biol Chem* 2004; **279:** 27194–27198.
10. Milanesi R, Baruscotti M, Gnecchi-Ruscone T, DiFrancesco D. Familial sinus bradycardia associated with a mutation in the cardiac pacemaker channel. *N Engl J Med* 2006; **354:** 151–157.
11. Nof E, Luria D, Brass D, Marek D, Lahat H, Reznik-Wolf H, et al. Point mutation in the HCN4 cardiac ion channel pore affecting synthesis, trafficking, and functional expression is associated with familial asymptomatic sinus bradycardia. *Circulation* 2007; **116:** 463–470.
12. Schulze-Bahr E, Neu A, Friederich P, Kaupp UB, Breithardt G, Pongs O, et al. Pacemaker channel dysfunction in a patient with sinus node disease. *J Clin Invest* 2003; **111:** 1537–1545.
13. Nakajima T, Wu J, Kaneko Y, Ashihara T, Ohno S, Irie T, et al. KCNE3 T4A as the genetic basis of Brugada-pattern electrocardiogram. *Circ J* 2012; **76:** 2763–2772.
14. Vallin H, Edhag O. Associated conduction disturbances in patients with symptomatic sinus node disease. *Acta Med Scand* 1981; **210:** 263–270.
15. Kudo M. A study of atrioventricular nodal function in patients with the sick sinus syndrome. *Jpn Circ J* 1979; **43:** 893–905.
16. Rubenstein JJ, Schulman CL, Yurchak PM, DeSanctis RW. Clinical spectrum of the sick sinus syndrome. *Circulation* 1972; **46:** 5–13.
17. Sakai Y, Imai S, Sato Y, Yagi H, Kushiro T. Clinical and electrophysiological characteristics of binodal disease. *Circ J* 2006; **70:** 1580–1584.
18. Habuchi Y, Han X, Giles W. Comparison of the hyperpolarization-activated and delayed rectifier currents in rabbit atrioventricular node and sinoatrial node. *Heart Vessels* 1995; **9:** 203–206.
19. Munk AA, Adjemian RA, Zhao J, Ogbaghebriel A, Shrier A. Electrophysiological properties of morphologically distinct cells isolated from the rabbit atrioventricular node. *J Physiol* 1996; **493:** 801–818.
20. Dobrzynski H, Nikolski VP, Sambelashvili AT, Greener ID, Yamamoto M, Boyett MR, et al. Site of origin and molecular substrate of atrioventricular junctional rhythm in the rabbit heart. *Circ Res* 2003; **93:** 1102–1110.
21. Crick SJ, Wharton J, Sheppard MN, Royston D, Yacoub MH, Anderson RH, et al. Innervation of the human cardiac conduction system. A quantitative immunohistochemical and histochemical study. *Circulation* 1994; **89:** 1697–1708.
22. DiFrancesco D. The onset and autonomic regulation of cardiac pacemaker activity: Relevance of the f current. *Cardiovasc Res* 1995; **29:** 449–456.
23. Chow LT, Chow SS, Anderson RH, Gosling JA. Autonomic innervation of the human cardiac conduction system: Changes from infancy to senility--an immunohistochemical and histochemical analysis. *Anat Rec* 2001; **264:** 169–182.
24. Kurokawa J, Furukawa T. Region- and condition-dependence of the membrane and Ca^{2+} clocks in the sinus node. *Circ J* 2012; **76:** 293–294.
25. Barbuti A, Terragni B, Brioschi C, DiFrancesco D. Localization of f-channels to caveolae mediates specific beta2-adrenergic receptor modulation of rate in sinoatrial myocytes. *J Mol Cell Cardiol* 2007; **42:** 71–78.

A novel *KCNQ1* missense mutation identified in a patient with juvenile-onset atrial fibrillation causes constitutively open I_{Ks} channels

Kanae Hasegawa, MD,[*†] Seiko Ohno, MD, PhD,[†] Takashi Ashihara, MD, PhD,[†] Hideki Itoh, MD, PhD,[†] Wei-Guang Ding, PhD,[‡] Futoshi Toyoda, PhD,[‡] Takeru Makiyama, MD, PhD,[§] Hisaaki Aoki, MD, PhD,[¶] Yoshihide Nakamura, MD, PhD,[¶] Brian P. Delisle, PhD,[‖] Hiroshi Matsuura, MD, PhD,[‡] Minoru Horie, MD, PhD[†]

From the [*]Department of Cardiovascular Biology and Medicine, Niigata University School of Medical and Dental Sciences, Niigata, Japan, [†]Department of Cardiovascular and Respiratory Medicine, Shiga University of Medical Science, Otsu, Japan, [‡]Department of Physiology, Shiga University of Medical Science, Otsu, Japan, [§]Department of Cardiovascular and Medicine, Kyoto University Graduate School of Medicine, Kyoto, Japan, [¶]Department of Pediatrics, Kinki University Faculty Medicine, Osaka, Japan, and [‖]Department of Physiology, University of Kentucky, Lexington, Kentucky.

BACKGROUND Atrial fibrillation (AF) is one of the most common cardiac arrhythmias. In some patients, the disease is inheritable; however, hereditary aspects of AF remain not fully elucidated.

OBJECTIVE The purpose of this study was to identify genetic backgrounds that contribute to juvenile-onset AF and to define the mechanism.

METHODS In 30 consecutive juvenile-onset AF patients (onset age <50 years), we screened AF-related genes (*KCNQ1, KCNH2, KCNE1-3, KCNE5, KCNJ2, SCN5A*). We analyzed the function of mutant channels using whole-cell patch-clamp techniques and computer simulations.

RESULTS Among the juvenile-onset AF patients, we identified three mutations (10%): *SCN5A*-M1875T, *KCNJ2*-M301K, and *KCNQ1*-G229D. Because *KCNQ1* variant (G229D) identified in a 16-year-old boy was novel, we focused on the proband. The G229D-I_{Ks} was found to induce a large instantaneous activating component without deactivation after repolarization to −50 mV. In addition, wild-type (WT)/G229D-I_{Ks} (WT and mutant coexpression) displayed both instantaneous and time-dependent activating currents. Compared to WT-I_{Ks}, the tail current densities in WT/G229D-I_{Ks} were larger at test potentials between −130 and −40 mV but smaller at test potentials between 20 and 50 mV. Moreover, WT/G229D-I_{Ks} resulted in a negative voltage shift for current activation (−35.2 mV) and slower deactivation. WT/G229D-I_{Ks} conducted a large outward current induced by an atrial action potential waveform, and computer simulation incorporating the WT/G229D-I_{Ks} results revealed that the mutation shortened atrial but not ventricular action potential.

CONCLUSION A novel *KCNQ1*-G229D mutation identified in a juvenile-onset AF patient altered the I_{Ks} activity and kinetics, thereby increasing the arrhythmogenicity to AF.

KEYWORDS Atrial fibrillation; Juvenile-onset atrial fibrillation; Ion channel; I_{Ks}; KCNQ1

ABBREVIATIONS **AF** = atrial fibrillation; **AP** = action potential; **CHO** = Chinese hamster ovary; **ECG** = electrocardiogram; **QTc** = corrected QT interval; **WT** = wild type

(Heart Rhythm 2014;11:67–75)

Introduction

Atrial fibrillation (AF) is the most prevalent cardiac rhythm abnormality and one of the major causes of morbidity and mortality.[1] Many risk factors predispose to AF, such as advancing age, male sex, structural heart disease, hypertension, obesity, diabetes mellitus, and hyperthyroidism.[1] In some patients, AF occurs in the absence of these risk factors; this subtype is called lone AF.[2] Genetic backgrounds have been shown to be associated with lone AF.[3] In fact, mutations in genes encoding ion channels,[4–11] gap junction proteins,[12] and signaling molecules[13] have been identified in families with AF and in isolated AF cases.[14] In 2003, Chen et al[4] first revealed among these AF-related genes the link between AF and a *KCNQ1* mutation (a gene encodes the slowly activating component of delayed rectifier K^+ current I_{Ks}). They reported a missense *KCNQ1* mutation, S140G, in familial AF, which showed a gain-of-function effect of I_{Ks}.[4,15]

This work was supported by Grants-in-Aid in Scientific Research from the Ministry of Education, Culture, Science, and Technology of Japan; a Health Sciences Research Grant from the Ministry of Health, Labour and Welfare of Japan; and Translational Research Funds from the Japan Circulation Society. **Address reprint requests and correspondence:** Dr. Minoru Horie, Department of Cardiovascular and Respiratory Medicine, Shiga University of Medical Science, Seta Tsukinowa-cho, Otsu 520-2192, Japan. E-mail address: horie@belle.shiga-med.ac.jp.

1547-5271/$-see front matter http://dx.doi.org/10.1016/j.hrthm.2013.09.073

To date, seven *KCNQ1* mutations have been reported to be associated with AF by exerting a gain-of-function effect with enhanced I_{Ks} current density with or without altered gating.[4,16–21] In addition, five of seven *KCNQ1* mutations (S140G, V141M, S209P, R231C, R231H) were identified in juvenile-onset AF patients. Among these five mutations, S140G, R231C, and R231H mutations were associated with QT prolongation. Regarding other mutations in genes that encode ion channels, functional analyses of the mutations have demonstrated either gain-of-function effects, for example, in *SCN5A* and *KCNJ2*,[5,6] or loss-of-function effects in *SCN5A* and *KCNA5*.[10,11] Intriguingly, these functional alterations are similar to those found in electrophysiologic remodeling in chronic AF.[22]

In order to clarify the genetic basis of juvenile-onset AF, we screened 30 consecutive probands for mutations in *KCNQ1, KCNH2, KCNE1-3, KCNE5, KCNJ2,* and *SCN5A*. Three heterozygous mutations were identified in *SCN5A*, *KCNJ2*, and *KCNQ1* in three probands from unrelated families (10%). We previously reported the former two mutations *SCN5A*-M1875T and *KCNJ2*-M301K.[5,6] The third missense *KCNQ1* mutation, G229D, was identified in a 16-year-old boy with AF, and it is novel. We examined the molecular mechanism underlying the *KCNQ1* mutation found in juvenile-onset AF by using a heterologous expression. We then incorporated the functional impact of the mutation into computational simulations of the atrial action potential (AP), and we found that it could contribute to shortening of the atrial AP duration leading to the arrhythmogenicity of AF.

Methods

Study subjects

The study was approved by the Institutional Ethics Committees of our institutes, and all patients provided informed consent. Thirty consecutive AF probands who developed AF at age <50 years were included in the study.

DNA isolation and genetic analysis

Genomic DNA was isolated from blood lymphocytes and screened for the entire open reading frames of *KCNQ1, KCNH2, KCNE1-3, KCNE5, KCNJ2,* and *SCN5A*. Genetic screening (except for *KCNJ2*) was performed using denaturing high-performance liquid chromatography (dHPLC WAVE System, Transgenomic, Omaha, NE, USA). Abnormal conformers and *KCNJ2* were amplified via polymerase chain reaction, and sequencing was performed using an ABI PRISM3130 DNA sequencer (Applied Biosystems, Wellesley, MA, USA). When a mutation was detected, we examined its presence in >200 Japanese healthy individuals to exclude the possibility of polymorphisms. When a mutation was detected in a proband, we checked whether or not his or her family members were also carriers.

In vitro mutagenesis

Full-length cDNA encoding human wild-type (WT) KCNQ1 (GenBank AF000571) in a pCI vector was subcloned into a pIRES2-EGFP expression vector. We engineered *KCNQ1*-G229D mutant using a site-directed mutagenesis kit (QuikChange II XL, Stratagene, La Jolla, CA, USA). The presence of mutations was confirmed by sequencing. Full-length cDNA encoding human KCNE1 (GenBank M26685) subcloned into the pCDNA3.1 expression vector was obtained by polymerase chain reaction from human heart cDNA library (Clontech Laboratories, Mountain View, CA, USA).

Electrophysiologic experiments

To assess the functional modulation by *KCNQ1* mutation, we used a heterologous expression system with the Chinese hamster ovary (CHO) cell line. Briefly, the cells were transiently transfected with *KCNQ1*-WT (0.5 μg) or *KCNQ1*-G229D (0.5 μg) or *KCNQ1*-WT (0.25 μg)/G229D (0.25 μg), and *KCNE1* (0.5 μg) plasmid DNA using Lipofectamine (Invitrogen Life Technologies, Carlsbad, CA, USA). For electrophysiologic experiments, after 48 hours of transfection, cells attached to glass coverslips were transferred to a 0.5-mL bath chamber perfused with extracellular solution at 1 to 2 mL/min. The chamber was mounted on the stage of an inverted microscope (ECLIPSE TE2000-U, Nikon, Tokyo, Japan) and maintained at 37°C. Patch-clamp experiments were conducted on GFP-positive cells.

Whole-cell membrane currents were recorded with an EPC-8 patch-clamp amplifier (HEKA Electronik, Lambrecht, Germany). Pipettes were prepared from glass capillary tube (Narishige, Tokyo, Japan) using a Sutter P-97 micropipette puller (Navato, CA, USA), and the tips were fire-polished with a microforge. Pipette resistance ranged from 2.5 to 3.5 MΩ. Pipettes were filled with a solution containing the following (in mM): 70 potassium aspartate, 40 KCl, 10 KH_2PO_4, 1 $MgSO_4$, 3 Na_2-ATP (Sigma, St. Louis, USA), 0.1 Li_2-GTP (Roche Diagnostics GmbH, Mannheim, Germany), 5 EGTA, and 5 HEPES; and pH was adjusted to 7.2 with KOH. The extracellular solution contained the following (in mM): 140 NaCl, 5.4 KCl, 1.8 $CaCl_2$, 0.5 $MgCl_2$, 0.33 NaH_2PO_4, 5.5 glucose, and 5.0 HEPES; pH was adjusted to 7.4 with NaOH. Liquid junction potential between the test solution and the pipette solution was measured to be around –10 mV and was corrected. HMR1556 (kind gift from Drs. H.J. Lang and J. Punter, Aventis Pharma Deutschland GmbH), a selective I_{Ks} blocker, was added from 10 mM stock solution in DMSO to the external solution (final DMSO concentration did not exceed 0.01%).

I_{Ks} was elicited by depolarizing voltage steps from a holding potential of –80 mV to various test potentials. I_{Ks} amplitude was determined by measuring the amplitude of the tail current elicited on repolarization to –50 mV following 2-second depolarization to 30 mV every 15 seconds and divided by the cell membrane capacitance to obtain current densities (pA/pF). I_{Ks} activation was evaluated by fitting the current–voltage relationship of the tail currents to a Boltzmann equation:

$$I_{Ktail} = 1/(1+\exp((V_h - V_m)/k))$$

where I_{Ktail} is the current amplitude density, V_h is the voltage at half-maximal activation, V_m is the test potential, and k is the

slope factor. Time constants for deactivation (tau_{fast} and tau_{slow}) were obtained by fitting a two-exponential function as follows:

$$I(t) = A_{fast}\exp(-t/tau_{fast}) + A_{slow}\exp(-t/tau_{slow}) + A_0$$

where I(t) is the current amplitude at time t, A_{fast}, A_{slow}, and A_0 are constants, and tau refers to the deactivation at the tail potential.

For voltage-clamp recordings using an atrial AP waveform, we applied a waveform generated from a computer simulation of an atrial AP at 1 Hz and recorded currents at 37°C.[21] Resting membrane potential in the CHO cell was determined by current clamp after creating the whole-cell configuration.

Computer simulation

To confirm the role of the *KCNQ1*-G229D mutation, we conducted simulations of paced activation in atrial and ventricular myocytes and of paced propagation in a one-dimensional (1D) bidomain ventricular myocardial model of 9.0-mm length with transverse conductivity, mimicking a transmural section of the left ventricular free wall. Membrane kinetics of the myocytes were represented by the Courtemanche human atrial model[23] and O'Hara-Rudy human ventricular model,[24] of which I_{Ks} models were replaced by the following equations based on WT-I_{Ks} or WT/G229D-I_{Ks} obtained by electrophysiologic recordings.

For both WT-I_{Ks} and WT/G229D-I_{Ks}:

$$I_{Ks} = G_{Ks}\cdot(1+0.6/(1+(3.8\cdot10^{-5}/[Ca^{2+}]_i)^{1.4}))\cdot x_{s1}\cdot x_{s2}\cdot(V_m - E_{Ks})$$

$$dx_{s1}/dt = (x_{s,\infty} - x_{s1})/tau_{X,s1}$$

$$dx_{s2}/dt = (x_{s,\infty} - x_{s2})/tau_{X,s2}$$

For WT-I_{Ks}:

$$x_{s,\infty} = 1/(1+\exp(-(V_m+28.8)/15.45))$$

$$tau_{x,s1} = 326.9 + 0.4/(2.326\cdot10^{-4}\cdot\exp((V_m+65.5)/17.8)) + 1.292\cdot10^{-3}\cdot\exp(-(V_m+227.2)/230))$$

$$tau_{x,s2} = 5/(0.01\cdot\exp((V_m-50)/100) + 0.0193\cdot\exp(-(V_m+66.54)/155))$$

For WT/G229D-I_{Ks}:

$$x_{s,\infty} = 0.85/(1+\exp(-(V_m+82.8)/41.72))$$

$$tau_{x,s1} = 326.9 + 0.4/(2.326\cdot10^{-4}\cdot\exp((V_m+119.5)/17.8)) + 1.292\cdot10^{-3}\cdot\exp(-(V_m+281.2)/230))$$

$$tau_{x,s2} = 5/(0.01\cdot\exp((V_m-50)/100) + 0.0193\cdot\exp(-(V_m+66.54)/155))$$

where G_{Ks} (mS/μF) is the maximum conductance of I_{Ks}; $[Ca^{2+}]_i$ (mM) is the intracellular Ca^{2+} concentration; x_{s1} and x_{s2} are the activation and deactivation gates, respectively, for I_{Ks}; V_m (mV) is the transmembrane potential; E_{Ks} (mV) is the reversal potential for I_{Ks}; $x_{s,\infty}$ is the steady-state value of both x_{s1} and x_{s2} gates; and $tau_{x,s1}$ and $tau_{x,s1}$ are the time constant of x_{s1} and x_{s2} gates, respectively. The values of G_{Ks} for atrial and ventricular models were 0.0136 and 0.0034 mS/μF, respectively, because the WT-I_{Ks} with these values faithfully reproduced the same current amplitudes as the original I_{Ks} models.[23,24]

To obtain the ventricular transmural gradient, we defined endocardial, midmyocardial, and epicardial layers of thickness (0.6, 6.0, and 2.4 mm, respectively[25]) and then incorporated transmural differences in ion channels and intracellular Ca^{2+} dynamics according to the original code.[24] Pacing stimuli of 2-ms duration and strength twice diastolic threshold were applied transmembranously to the endocardial end at a cycle length of 1000 ms. To obtain ECGs similar to those recorded from left precordial leads, a unipolar recording electrode was located 2 cm above the epicardial end of the tissue. Transmural conductivity in the extracellular space was set to 2.36 mS/cm and that in the intracellular space for endocardial and midmyocardial layers and for epicardial layer were set to 0.38 and 0.29 mS/cm, respectively.[26] Other model parameters and the numerical approach have been described elsewhere.[25]

Statistical analysis

All data are given as mean ± SEM. Differences between two groups were examined by independent Student *t* test. $P < .05$ was considered significant.

Results

Genetic analysis

We identified three heterozygous mutations in 3 of 30 probands with juvenile-onset AF (10%): *SCN5A*-M1875T, *KCNJ2*-M301K, and *KCNQ1*-G229D. Details of patients with *SCN5A*-M1875T and *KCNJ2*-M301K have been reported previously.[5,6] The third *KCNQ1* mutation, a single-base substitution at nucleotide 686 (c.686G > A),

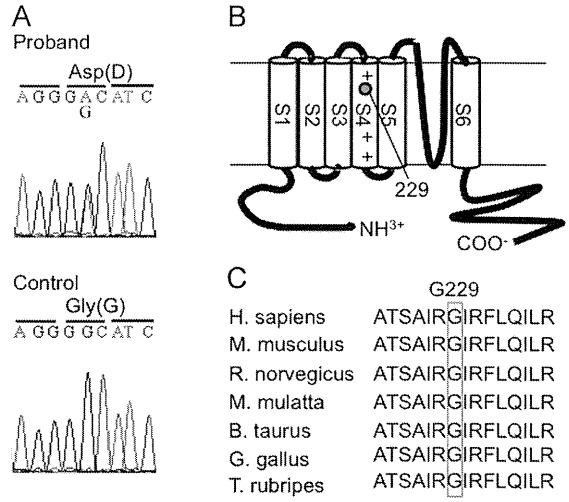

Figure 1 Genetic analysis of the proband. **A:** Electropherograms of *KCNQ1* gene showing a mutation, p.G229D (c.686G > A) in the proband. **B:** Topology of Kv7.1 encoded by KCNQ1. G229 is located in the fourth transmembrane segment (S4), known as the voltage sensor. **C:** Alignment of Kv7.1 sequence showing conservation of glycine at position 229 (G229) across species.

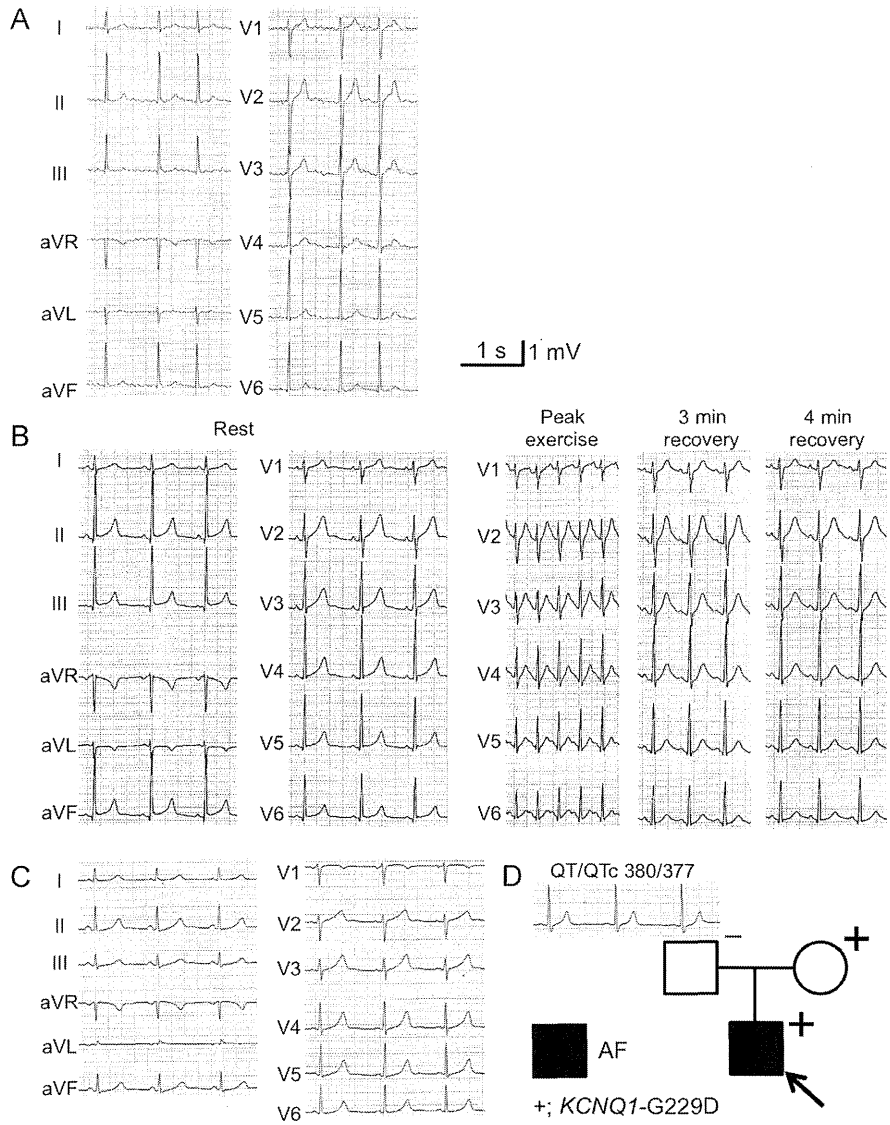

Figure 2 Clinical characteristics. Twelve-lead ECGs of the proband, indicating atrial fibrillation (AF) at the first detection **(A)** and sinus rhythm at rest and during exercise tolerance test after catheter ablation **(B). C:** ECG of the proband's mother. **D:** Pedigree and ECG (V_5 lead) of the proband's father. Males and female are represented as *squares* and *circle*, respectively. *Arrow* indicates the proband. +/– symbols indicate the presence/absence of the *KCNQ1*-G229D variant. *Filled symbols* indicate the development of AF.

causes an amino acid change from glycine to aspartic acid at position 229 in the Kv7.1 potassium channel (Figure 1A). Gly-229 resides in the fourth transmembrane segment (S4), which is known as a voltage sensor (Figure 1B). Alignment of the Kv7.1 amino acid sequence (Figure 1C) demonstrated that the glycine at position 229 is conserved in several species, suggesting its importance at this position. G229D was absent in 400 Japanese control alleles and has not been reported according to the NHLBI Exome Sequencing Project (ESP), Exome Variant Server (http://evs.gs.washington.edu/EVS/). In the proband, we did not find any mutations in other candidate genes described in the Methods.

Clinical characteristics

KCNQ1-G229D mutation was identified in a 16-year-old boy who was diagnosed as AF at the age of 16 (QT/QTc [corrected QT interval] 380/429 ms; Figure 2A). Cardiovascular and blood examination including thyroid hormone were all normal. He took propranolol hydrochloride 30 mg/day and digoxin 0.125 mg/day for rate control and bepridil 100 mg/day for pharmacologic cardioversion, but they failed to maintain his sinus rhythm. Moreover, cardioversion did not restore sinus rhythm.

As the next step of treatment, he underwent radiofrequency catheter ablation therapy (pulmonary vein isolation). After the therapy, his AF did not recur without any antiarrhythmic agents for 20 months. Eighteen months after therapy, exercise tolerance test was performed (Figure 2B). The QTc interval both at rest and at 4 minutes of recovery after exercise showed borderline criteria of QT prolongation (QT/QTc from 415/452 ms to 372/480 ms).

The G229D mutation was also identified in the boy's asymptomatic mother. Her ECG at rest showed borderline

criteria of QT prolongation (QT/QTc 460/468 ms; Figure 2C). There was no family history of AF (Figure 2D).

Functional analysis

To elucidate the genetic effect of G229D mutant, we conducted functional characterization by using a heterologous expression system. As shown in Figure 3A, coexpression of *KCNQ1*-WT (0.5 μg) with *KCNE1* (0.5 μg) produced a slowly activating outward WT-I_{Ks} on depolarization to 30 mV from the holding potential of −80 mV. In contrast, transfection of *KCNQ1*-G229D (0.5 μg), coexpressed with equimolar *KCNE1*, produced an instantaneously activated G229D-I_{Ks} that did not deactivate after repolarization to −50 mV (Figure 3B). Moreover, the cells coexpressing WT and mutant (0.25 μg each) channels with *KCNE1* displayed both instantaneous (indicated by an arrow) and time-dependent activated WT/G229D-I_{Ks} with deactivation process (Figure 3C), suggesting that coexpression of WT results in an intermediate functional phenotype. HMR1556 (an I_{Ks} blocker; 1 μM) completely inhibited all conducted I_{Ks} currents (indicated by red traces in Figures 3A through 3C).

Activating currents were then divided into instantaneous and time-dependent components by measuring the instantaneous current level at 10 ms after the depolarization pulse and the time-dependent current as a difference between current level at 10 ms after depolarization and at the end of depolarizing duration (steady state (indicated by arrowhead in Figure 3C). As summarized in bar graphs of Figure 3D, instantaneous components of WT/G229D-I_{Ks} were 171.9 ± 28.3 pA/pF, which was significantly larger than those in WT-I_{Ks} (40.8 ± 14.1 pA/pF, $P < .001$). In contrast, time-

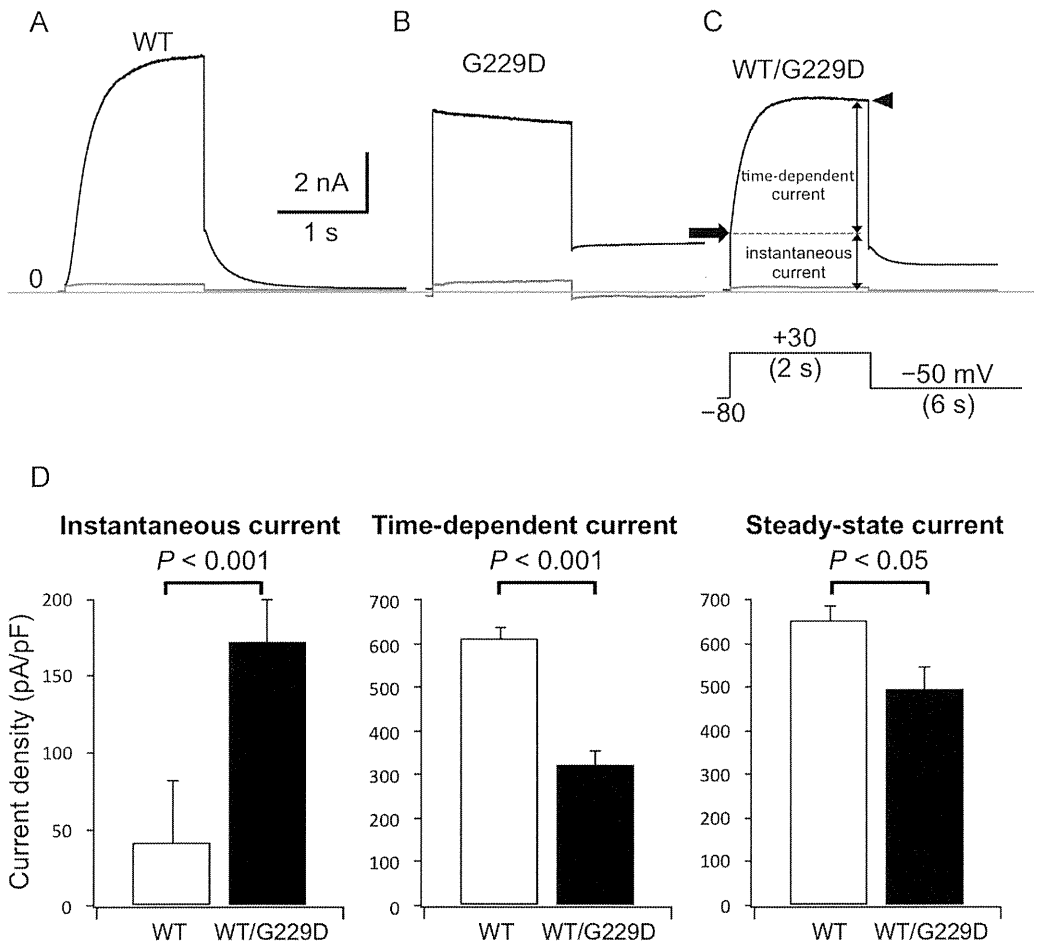

Figure 3 G229D mutation drastically alters properties of reconstituted I_{Ks} current. Whole-cell Kv7.1 currents recorded from CHO cells expressing wild type (WT; **A),** G229D **(B),** and WT/G229D **(C).** Current was elicited by 2-second voltage step from a holding potential of −80 mV to 30 mV before *(black trace)* and after *(red trace)* application of HMR 1556 (1 μM). *Blue lines* indicate the zero current level. *Inset (lower right)* shows the voltage application protocol. **D:** Bar graphs of current densities summarized from multiple experiments for instantaneous *(left),* time-dependent *(middle),* and steady-state *(right)* currents during voltage step to 30 mV. Instantaneous current level was measured 10 ms after depolarization *(arrow).* Time-dependent current was estimated as a difference between an instantaneous current level *(arrow)* and that at the end of depolarizing pulse (steady-state: *arrowhead*). *White bars* indicate data from WT (n = 19). *Black bars* indicate data from WT/G229D (n = 19).

dependent and steady-state currents were significantly larger in WT-I_{Ks} than WT/G229D-I_{Ks} (Figures 3C and 3D).

Figures 4A depicts two families of I_{Ks} current traces elicited by 2-second depolarizing voltage-clamp steps from a holding potential of –80 mV to various test potentials and following repolarization to –50 mV (inset shows voltage-step protocol): left, WT-I_{Ks} and right, WT/G229D-I_{Ks}. Again, WT/G229D-I_{Ks} displayed an instantaneous activation (indicated by arrow in Figure 4A), which was followed by time-dependent slow activation (intermediate phenotype). On repolarization to –50 mV, tail currents did not completely deactivate. As shown in the lower panels, both WT and WT/G229D currents were entirely inhibited by HMR1556 (1 μM).

Figures 4B shows peak tail current–voltage relationships for WT-I_{Ks} and WT/G229D-I_{Ks} obtained from multiple experiments. Tail current densities were larger at test potentials between –130 and –40 mV in WT/G229D (filled circles) than in WT (open circles). At more depolarizing test pulses (20 to 50 mV), however, they were reversely smaller in WT/G229D than in WT.

In Figure 4C, voltage-dependent activations of WT and WT/G229D tail currents were evaluated by fitting to a Boltzmann equation. In WT/G229D, the voltage dependence for I_{Ks} activation was significantly shifted to more hyperpolarized potentials (from –15.1 ± 1.4 mV to –50.8 ± 7.8 mV).

Because deactivation of WT/G229D-I_{Ks} was extremely slow at –50 mV (Figures 3C and 4A), in the following experiments (Figure 5A) we measured deactivation kinetics (tau_{fast} and tau_{slow}) at –120 mV after 2-second depolarization to 30 mV (left trace, WT; right trace, WT/G229D). As summarized in the bar graphs shown in Figure 5B, compared to WT, rates for deactivation in WT/G229D were significantly slower (tau_{fast} 77.3 ± 3.6 ms vs 115.0 ± 8.9 ms; tau_{slow} 270.9 ± 124.9 ms vs 1716.3 ± 110.9 ms).

In the next series of experiments, we used an atrial AP waveform to elicit current activation. WT/G229D-I_{Ks} thus conducted large outward currents (Figure 6A, red trace). As summarized in the bar graphs shown in Figure 6B, integral current densities were significantly larger in WT/G229D than WT, suggesting a gain-of-function effect by G229D mutation.

Because the instantaneous current component of WT/G229D-I_{Ks} could influence the resting membrane potential, we measured the resting potential of CHO cells expressing various constructs (Figure 6C). Resting membrane potentials were –4.6 ± 1.9 mV in nontransfected cells and –41.3 ± 2.2 mV in cells expressing WT channels. In contrast, those

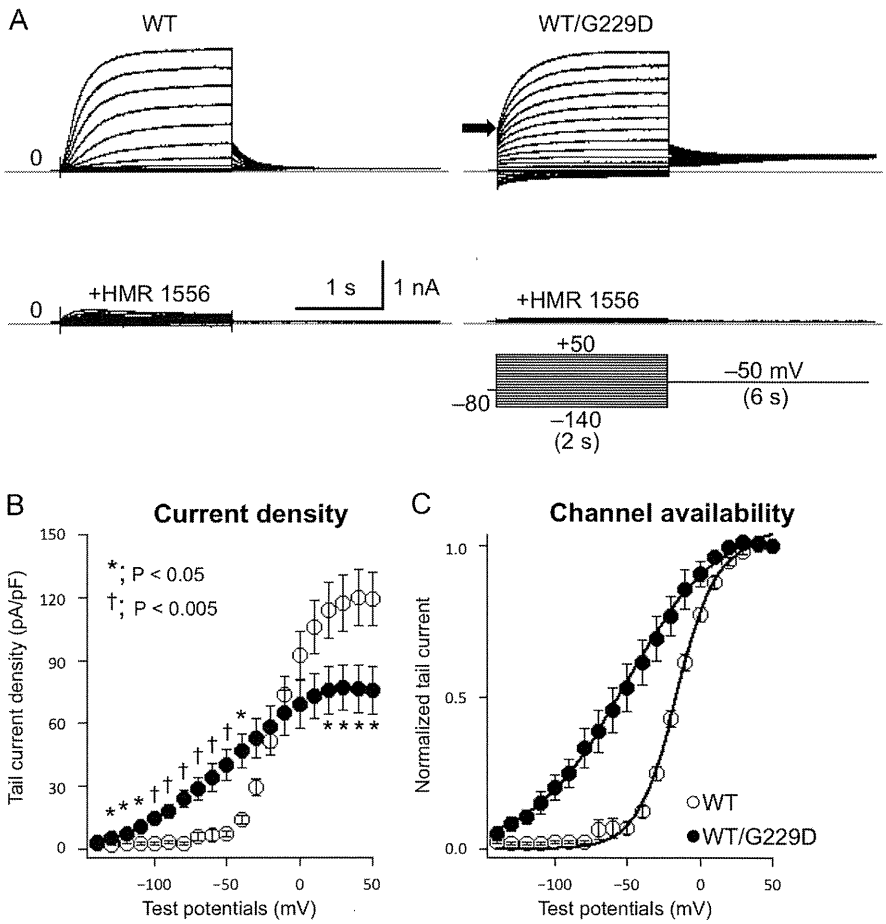

Figure 4 Electrophysiologic properties of wild type (WT) and WT/G229D. **A:** Two representative sets of current traces recorded from CHO cells expressing WT *(left)* and WT/G229D *(right)*. Currents were elicited by 2-second depolarizing voltage-clamp steps from a holding potential of –80 mV to various test potentials (from –140 to 50 mV) before *(top)* and after *(bottom)* application of HMR1556 (1 μM). *Arrow* in the *right panel* indicates the instantaneous current level at 50-mV test potential. *Blue lines* indicate the zero current level. *Inset (lower right)* shows the voltage application protocol. **B:** Tail current–voltage relationships for WT *(open circles,* n = 7) and WT/G229D *(filled circles,* n = 6). Tail current densities are plotted as a function of test potentials. *Vertical lines* through symbols indicate the standard error. **C:** Current–voltage relationships for normalized tail currents in WT *(open circles,* n = 7) and WT/G229D *(filled circles,* n = 6). *Vertical lines* through symbols indicate the standard error.

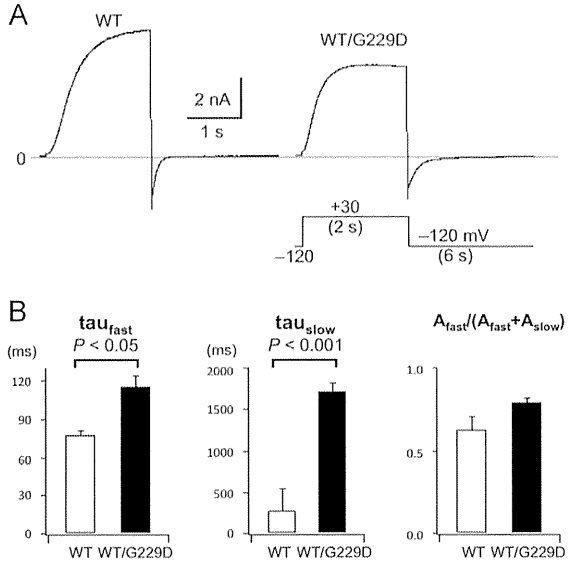

Figure 5 Coexpression with G229D slows down the deactivation process. **A:** Current traces from CHO cells expressing wild type (WT; *left*) and WT/G229D *(right).* Currents were elicited by a 2-second depolarizing voltage step to 30 mV followed by repolarization to −120 mV to obtain a completely deactivated tail current. *Blue line* indicates the zero current level. *Inset (lower right)* shows the voltage application protocol. **B:** Bar graphs showing averaged tau_{fast} *(left),* tau_{slow} *(middle),* and $A_{fast}/(A_{fast} + A_{slow})$ *(right). White bars* indicate data from WT (n = 8). *Black bars* indicate date from WT/G229D (n = 10).

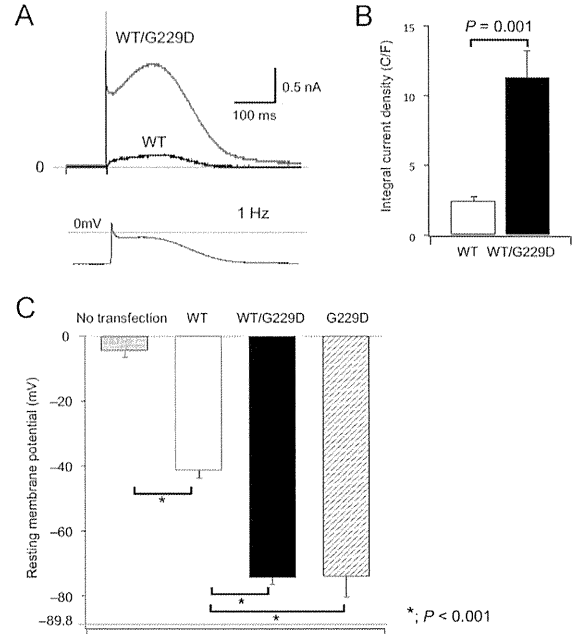

Figure 6 **A, B:** Atrial action potential clamp recording. **A:** Whole-cell clamp was conducted by using an atrial action potential waveform (indicated in *inset* below the traces). Two representative current traces recorded from cells expressing WT *(black trace)* and WT/G229D *(red trace). Blue line* indicates the zero current level. **B:** Bar graph showing averaged integral current densities measured by the area enclosed by the current curves. *White bar* indicates data from WT (n = 10). *Black bar* indicates data from WT/G229D (n = 11). **C:** Bar graph showing averaged resting membrane potentials from CHO cells under four different conditions: no transfection of constructs (*dot bar,* n = 23), transfected with WT (*white bar,* n = 25), WT/G229D (*black bar,* n = 15), and G229D (*striped bar,* n = 12). *Blue line* indicates the equilibrium potential of potassium ion in the present experimental condition.

expressing WT/G229D or G229D channels showed significantly more negative resting potentials (–74.6 ± 1.9 mV and –74.3 ± 6.2 mV), which were closer to the calculated equilibrium potential of potassium ion (–89.9 mV in the present experimental condition). Therefore, the negative shift of resting potentials may be due to constitutive opening of WT/G229D or G229D channels.

Computer simulation

To explore the cellular mechanisms by which the G229D mutation manifested AP shortening in atrial but not ventricular myocytes, we performed a computer simulation study by using both atrial and ventricular myocytes and 1D myocardial model (Figure 7). Based on the I_{Ks} obtained by electrophysiologic recording (Figures 4 and 5), we numerically reproduced both WT and WT/G229D current traces (Figure 7A), the current–voltage relationship curves (Figure 7B), and the normalized activation curves (Figure 7C). The numerically reproduced I_{Ks} were incorporated into the human atrial and ventricular myocyte models (Figures 7D and E, respectively). WT/G229D-I_{Ks} was markedly larger than WT-I_{Ks} in both atrial and ventricular cell models. Because of the difference in the contribution of I_{Ks} to AP formation, the mutation markedly shortened AP duration in the atrial but not the ventricular myocyte model. Indeed, the numerically reproduced I_{Ks} did not shorten the QT interval in the 1D model under 1-Hz pacing (Figure 7F), consistent with the ECG phenotype of the proband.

Discussion

In the present study, we described a novel missense *KCNQ1* mutation, G229D, in a juvenile-onset AF patient. The proband's AF, which started at the age of 16 years, was refractory to bepridil. Radiofrequency catheter ablation therapy was effective in maintaining his sinus rhythm. In sinus rhythm, he showed borderline QT prolongation. His mother carried the same heterozygous mutation and also showed borderline QT prolongation.

G229D mutant I_{Ks} reconstituted in CHO cells displayed unique functional properties: a time-independent component (instantaneous current) and slow deactivation. In detail, (1) instantaneous component of WT/G229D was significantly larger than that of WT; (2) the tail current density of WT/G229D was larger at test potentials between –130 and –40 mV; (3) WT/G229D produced a negative shift in the voltage dependence of half-maximal activation (–35.2 mV); (4) the deactivation of WT/G229D was significantly slower than that of WT; (5) a large integral current density of WT/G229D was indeed induced by the atrial AP clamp experiment; and (6) computational AP simulations suggest WT/G229 selectively shortens the atrial AP. Taken together, these results are

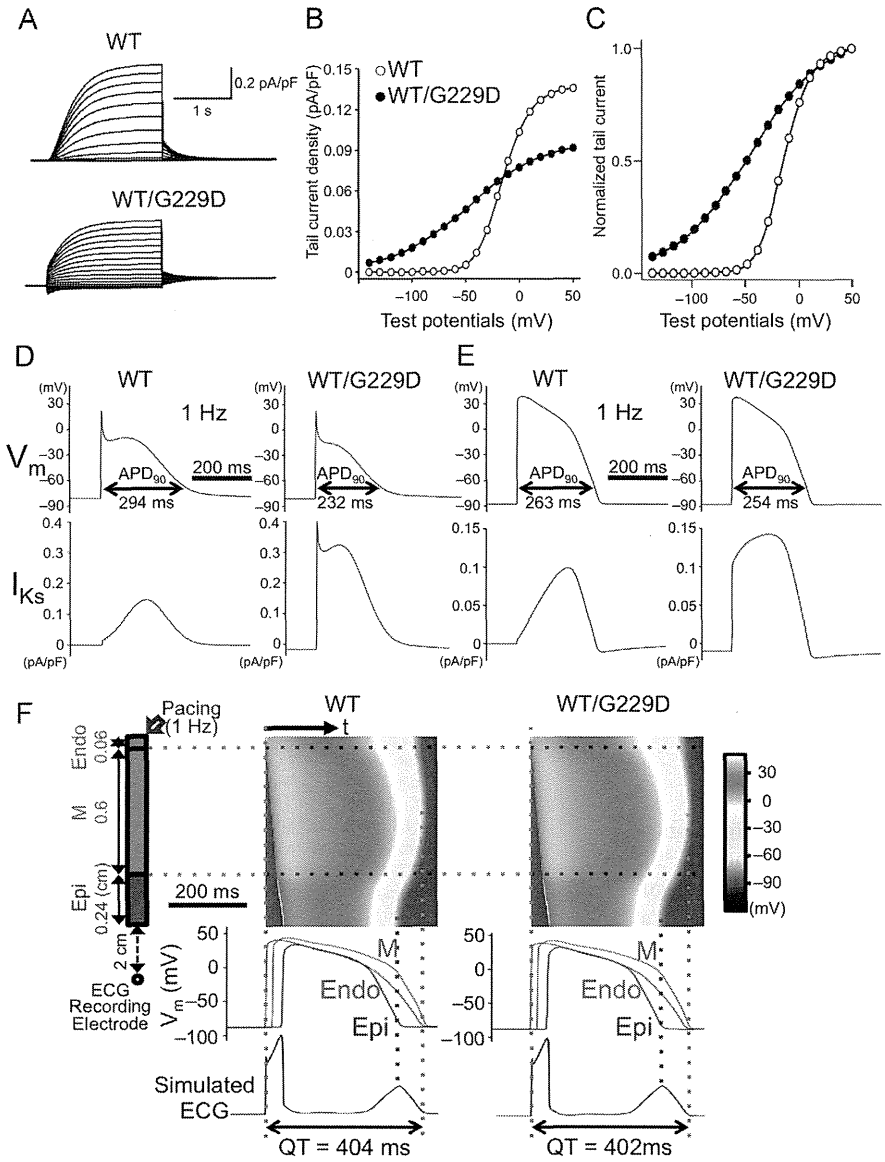

Figure 7 Computer simulation study using both atrial and ventricular myocytes and one-dimensional (1D) myocardial model. Numerically reproduced current traces **(A),** tail current–voltage relationships **(B)** and normalized activation curves **(C)** of wild-type (WT) model *(open circles)* and WT/G229D model *(filled circles).* **D:** Atrial action potential (AP) and I_{Ks} in the computer models of human atrial myocyte with WT-I_{Ks} or WT/G229D-I_{Ks}. **E:** Ventricular AP and I_{Ks} in the computer models of human ventricular myocyte with WT-I_{Ks} or WT/G229D-I_{Ks}. **F:** Transmural heterogeneity of AP and the simulated ECG in the 1D ventricular model.

consistent with a view that the mutation caused gain-of-function effects on I_{Ks}, thereby shortening atrial refractoriness and increasing susceptibility to AF.

Regarding *KCNQ1* mutations associated with juvenile-onset AF, five mutations (S140G, V141M, S209P, R231C, R231H) were previously identified.[4,16,19–21] Chen et al[4] first reported the *KCNQ1*-S140G mutation that potentiated I_{Ks}, especially the component of instantaneous activation. Later in 2005, Hong et al[16] reported the *KCNQ1*-V141M mutation in a baby with AF and an abnormally short QT interval. They also described a large instantaneous activation of V141M-I_{Ks}. Das et al[19] then reported a heterozygous *KCNQ1*-S209L mutation. This mutation also showed an instantaneous opening when expressed as WT/S209L-I_{Ks}, a significantly negative shift of half-maximal activation voltage (–42.4 mV), and slow current deactivation.

More recently, Bartos et al[20,21] reported *KCNQ1*-R231C and R231H mutations in families with AF and mild QT prolongation. These mutations showed marked instantaneous activation and significantly negative shift in half-maximal activation (–30 to –40 mV). In addition, recent extensive mutagenesis experiments and the structural model of KCNQ1 protein[15] suggest that residues S140, E160, R237, and R231 closely associate with one another in the closed state. Substitution of amino acid at any of the charged S140, E160, R237, or R231 residues was shown to disrupt KCNQ1 deactivation ("lock" the I_{Ks} channel in the open state).[15,20] This suggests that these residues are critical for

normal KCNQ1 channel closing and that G229D might also disrupt the interaction among these residues.

Our biophysical assessment revealed that the function of G229D resembled that of R231C and R231H mutations,[20,21] which reside near glycine at 229. However, the G229D mutation was somewhat different in that it caused a borderline QT prolongation. Indeed, it appeared not to affect the ventricular AP while markedly shortening the atrial AP. Our computer simulation 1D model (Figure 7F) partially explained these apparently different effects of G229D for the first time. Regarding the pharmacologic treatment of AF in the proband, a low concentration of pure I_{Ks} blocker would be a potential for restoring sinus rhythm without considerable prolongation of QT interval. In fact, Courtney et al[27] recently reported the enhanced sensitivity of *KCNQ1* gain-of-function mutation (S140G) for HMR1556, a pure I_{Ks} blocker, compared to that of WT channels.

Study limitations

In the present study, we used a heterologous expression system to assess functional modulation by the *KCNQ1* mutation. However, the environment of this system is different from that of cardiac myocytes or whole heart. Therefore, our data might not always explain electrophysiologic modulation in the whole heart.

Conclusion

We identified a novel *KCNQ1*-G229D mutation in a patient with juvenile-onset AF. In the heterozygous condition, the mutation changed I_{Ks} channel kinetics and showed a gain-of-function modulation of I_{Ks}. In the computer simulation model, it markedly shortened the atrial AP duration, suggesting the tendency toward AF.

Acknowledgments

We are grateful to the Japanese juvenile-onset AF families for their willingness to participate in this study. We thank Dr. Daniel C. Bartos (Department of Physiology, University of Kentucky, Lexington, USA) for the AP waveform and Arisa Ikeda, Kazu Toyooka, and Aya Umehara for excellent technical assistance.

References

1. Kannel WB, Benjamin EJ. Status of the epidemiology of atrial fibrillation. Med Clin North Am 2008;92:17–40, ix.
2. Brand FN, Abbott RD, Kannel WB, Wolf PA. Characteristics and prognosis of lone atrial fibrillation. 30-year follow-up in the Framingham Study. JAMA 1985;254:3449–3453.
3. Sinner MF, Ellinor PT, Meitinger T, Benjamin EJ, Kaab S. Genome-wide association studies of atrial fibrillation: past, present, and future. Cardiovasc Res 2011;89:701–709.
4. Chen YH, Xu SJ, Bendahhou S, et al. KCNQ1 gain-of-function mutation in familial atrial fibrillation. Science 2003;299:251–254.
5. Makiyama T, Akao M, Shizuta S, et al. A novel SCN5A gain-of-function mutation M1875T associated with familial atrial fibrillation. J Am Coll Cardiol 2008;52:1326–1334.
6. Hattori T, Makiyama T, Akao M, et al. A novel gain-of-function KCNJ2 mutation associated with short-QT syndrome impairs inward rectification of Kir2.1 currents. Cardiovasc Res 2012;93:666–673.
7. Ravn LS, Aizawa Y, Pollevick GD, et al. Gain of function in I_{Ks} secondary to a mutation in KCNE5 associated with atrial fibrillation. Heart Rhythm 2008;5: 427–435.
8. Lundby A, Ravn LS, Svendsen JH, Hauns S, Olesen SP, Schmitt N. KCNE3 mutation V17M identified in a patient with lone atrial fibrillation. Cell Physiol Biochem 2008;21:47–54.
9. Yang Y, Xia M, Jin Q, et al. Identification of a KCNE2 gain-of-function mutation in patients with familial atrial fibrillation. Am J Hum Genet 2004;75:899–905.
10. Ellinor PT, Nam EG, Shea MA, Milan DJ, Ruskin JN, MacRae CA. Cardiac sodium channel mutation in atrial fibrillation. Heart Rhythm 2008;5:99–105.
11. Olson TM, Alekseev AE, Liu XK, et al. Kv1.5 channelopathy due to KCNA5 loss-of-function mutation causes human atrial fibrillation. Hum Mol Genet 2006;15:2185–2191.
12. Gollob MH, Jones DL, Krahn AD, et al. Somatic mutations in the connexin 40 gene (GJA5) in atrial fibrillation. N Engl J Med 2006;354:2677–2688.
13. Hodgson-Zingman DM, Karst ML, Zingman LV, et al. Atrial natriuretic peptide frameshift mutation in familial atrial fibrillation. N Engl J Med 2008;359: 158–165.
14. Mahida S, Lubitz SA, Rienstra M, Milan DJ, Ellinor PT. Monogenic atrial fibrillation as pathophysiological paradigms. Cardiovasc Res 2011;89:692–700.
15. Restier L, Cheng L, Sanguinetti MC. Mechanisms by which atrial fibrillation-associated mutations in the S1 domain of KCNQ1 slow deactivation of I_{Ks} channels. J Physiol 2008;586:4179–4191.
16. Hong K, Piper DR, Diaz-Valdecantos A, et al. De novo KCNQ1 mutation responsible for atrial fibrillation and short QT syndrome in utero. Cardiovasc Res 2005;68:433–440.
17. Lundby A, Ravn LS, Svendsen JH, Olesen SP, Schmitt N. KCNQ1 mutation Q147R is associated with atrial fibrillation and prolonged QT interval. Heart Rhythm 2007;4:1532–1541.
18. Otway R, Vandenberg JI, Guo G, et al. Stretch-sensitive KCNQ1 mutation A link between genetic and environmental factors in the pathogenesis of atrial fibrillation? J Am Coll Cardiol 2007;49:578–586.
19. Das S, Makino S, Melman YF, et al. Mutation in the S3 segment of KCNQ1 results in familial lone atrial fibrillation. Heart Rhythm 2009;6:1146–1153.
20. Bartos DC, Duchatelet S, Burgess DE, et al. R231C mutation in KCNQ1 causes long QT syndrome type 1 and familial atrial fibrillation. Heart Rhythm 2011;8:48–55.
21. Bartos DC, Anderson JB, Bastiaenen R, et al. A KCNQ1 mutation causes a high penetrance for familial atrial fibrillation. J Cardiovasc Electrophysiol 2013;24:562–569.
22. Bosch RF, Nattel S. Cellular electrophysiology of atrial fibrillation. Cardiovasc Res 2002;54:259–269.
23. Courtemanche M, Ramirez RJ, Nattel S. Ionic mechanisms underlying human atrial action potential properties: insights from a mathematical model. Am J Physiol 1998;275:H301–H321.
24. O'Hara T, Virag L, Varro A, Rudy Y. Simulation of the undiseased human cardiac ventricular action potential: model formulation and experimental validation. PLoS Comput Biol 2011;7:e1002061.
25. Tsuji-Wakisaka K, Akao M, Ishii TM, et al. Identification and functional characterization of KCNQ1 mutations around the exon 7-intron 7 junction affecting the splicing process. Biochim Biophys Acta 2011;1812:1452–1459.
26. Yamada KA, Kanter EM, Green KG, Saffitz JE. Transmural distribution of connexins in rodent hearts. J Cardiovasc Electrophysiol 2004;15:710–715.
27. Campbell CM, Campbell JD, Thompson CH, Vanoye CG, George AL Jr. Selective targeting of gain-of-function KCNQ1 mutations predisposing to atrial fibrillation. Circ Arrhythm Electrophysiol 2013;6:960–966.

Journal of Arrhythmia 30 (2014) 161–166

Contents lists available at ScienceDirect

Journal of Arrhythmia

journal homepage: www.elsevier.com/locate/joa

Original Article

A rare *KCNE1* polymorphism, D85N, as a genetic modifier of long QT syndrome

Kanae Hasegawa, MD[a], Seiko Ohno, MD, PhD[a], Hideki Itoh, MD, PhD[a], Takeru Makiyama, MD, PhD[b], Takeshi Aiba, MD, PhD[c], Yasutaka Nakano, MD, PhD[a], Wataru Shimizu, MD, PhD[d], Hiroshi Matsuura, MD, PhD[e], Naomasa Makita, MD, PhD[f], Minoru Horie, MD, PhD[a,*]

[a] *Department of Cardiovascular and Respiratory Medicine, Shiga University of Medical Science, Seta Tsukinowa-cho, Otsu 520-2192, Japan*
[b] *Department of Cardiovascular Medicine, Kyoto University Graduate School of Medicine, Kyoto, Japan*
[c] *Division of Arrhythmia and Electrophysiology, Department of Cardiovascular Medicine, National Cerebral and Cardiovascular Center, Suita, Japan*
[d] *Department of Cardiovascular Medicine, Nippon Medical School, Tokyo, Japan*
[e] *Department of Physiology, Shiga University of Medical Science, Otsu, Japan*
[f] *Department of Molecular Physiology, Nagasaki University Graduate School of Biomedical Sciences, Nagasaki, Japan*

ARTICLE INFO

Article history:
Received 11 April 2013
Received in revised form
19 July 2013
Accepted 26 August 2013
Available online 26 October 2013

Keywords:
Long QT syndrome
Single nucleotide polymorphism
Modifier

ABSTRACT

Background: The gene *KCNE1* encodes the β-subunit of cardiac voltage-gated K^+ channels and causes long QT syndrome (LQTS). LQTS is characterized by the prolongation of QT interval and lethal arrhythmias such as torsade de pointes (TdP). A *KCNE1* polymorphism, D85N, has been shown to modify the phenotype of LQTS through a loss-of-function effect on both KCNQ1 and KCNH2 channels when co-expressed and reconstituted in a heterologous expression system.
Methods: A screening for the D85N polymorphism was performed in 355 LQTS families with mutations in *KCNQ1*, *KCNH2*, or *SCN5A*. Among the probands who had a heterozygous status with the polymorphism, we focused on a family with a *KCNH2* mutation (E58K), a N-terminal missense mutation, and examined the clinical significance of this polymorphism. We also conducted biophysical assays to analyze the effect of the polymorphism in mammalian cells.
Results: In 355 probands, we found 14 probands (3.9%) who had a heterozygous compound status with the D85N polymorphism. In the family with a *KCNE1*-D85N polymorphism and a *KCNH2*-E58K mutation, the proband and her daughter carried both the *KCNH2* mutation and the *KCNE1*-D85N polymorphism. They experienced repetitive syncope and TdP. Two sons of the proband had either *KCNH2*-E58K mutation or *KCNE1*-D85N, but were asymptomatic. Biophysical assays of *KCNE1*-D85N with *KCNH2*-E58K variants produced a larger reduction in the reconstituted I_{Kr} currents compared to co-expression with wild-type *KCNE1*.
Conclusions: The *KCNE1*-D85N polymorphism modified the clinical features of LQTS patients.

1. Introduction

Long QT syndrome (LQTS) is characterized by cardiac repolarization abnormalities that lead to TdP, syncope, and sudden cardiac death [1]. The disease is genetically heterogeneous and caused by mutations in > 10 genes, including *KCNH2* and *KCNE1* [2–4]. In LQTS probands with heterozygous genetic variants, compound mutations usually exacerbate the disease severity compared to other family members who carry a single mutation [5–7]. Previously, the coexistence of the single nucleotide polymorphism (SNP) *KCNH2*-K897T with the latent *KCNH2* mutation A1116V was shown to modify the clinical symptoms [8].

A *KCNE1* C-terminal polymorphism, D85N, has been found in the normal population. The sequence, a nucleotide replacement from G to A at 253, causes an amino acid change from aspartic acid to asparagine at position 85 [9]. The allele frequency of the polymorphism is reported to be 0.7% in apparently healthy Asians [10]. Paulussen et al. demonstrated that the allele frequency of the same variant among Europeans is 5% in drug-induced LQTS patients who experienced TdP, but 0% in the control population [11]. More recently, we demonstrated that the D85N allele frequency is 0.8% among apparently healthy Japanese individuals and that it is significantly higher among clinically diagnosed LQTS probands (3.9%) [9]. In a patch-clamp experiment using a heterologous expression system in a mammalian cell line, *KCNE1*-D85N was found to reduce the current densities in *KCNQ1/KCNE1* channels (I_{Ks}) and *KCNH2/KCNE1* channels (I_{Kr}) by 28% and 31%, respectively [9].

In the present study, we screened for the D85N polymorphism in 355 LQTS probands in which we could identify a mutation in

Abbreviations: CHO cell, Chinese hamster ovary cell; LQTS, long QT syndrome; PPM, post pacemaker implantation; SCD, sudden cardiac death; SNP, single nucleotide polymorphism; TdP, torsade de pointes

* Corresponding author. Tel.: +81 77 548 2213; fax: +81 77 543 5839.
E-mail address: horie@belle.shiga-med.ac.jp (M. Horie).

1880-4276/$ - see front matter © 2013 Japanese Heart Rhythm Society. Published by Elsevier B.V. All rights reserved.
http://dx.doi.org/10.1016/j.joa.2013.08.004

KCNQ1, *KCNH2*, or *SCN5A*, and found 14 patients that carried the polymorphism in addition to a single pathologic LQTS-related gene mutation. Among them, in a family with *KCNH2*-E58K, D85N appeared to modulate the phenotype of family members. In order to clarify the phenotype–genotype correlation, we then conducted functional assays of the variants by using a heterologous expression system in Chinese hamster ovary (CHO) cells.

2. Material and methods

2.1. Genetic analysis

The cohort of this study was 355 LQTS probands who were identified as having mutations in *KCNQ1*, *KCNH2*, or *SCN5A* and their family members. Genetic analysis was performed after obtaining written informed consent in accordance with the study protocol approved by our institutional ethics committees. In addition to the 3 genes listed above, genetic screening for *KCNE1* was performed by single strand conformation polymorphism or denaturing high-performance liquid chromatography using a WAVE System Model 3500 (Transgenomic, Omaha, NE, USA). Abnormal conformers were amplified by polymerase chain reaction (PCR). Sequencing was performed with an ABI PRISM3130 DNA sequencer (Applied Biosystems, Wellesley, MA, USA).

2.2. Mutagenesis

Complementary deoxyribonucleic acid (cDNA) for human *KCNE1* (GenBank M26685) was kindly provided by Dr. J. Barhanin (Institut de Pharmacologie Moléculaire et Cellulaire, CNRS, Valbonne, France) and was subcloned into a pIRES-CD8 vector. cDNA for human *KCNH2* (GenBank AF363636) was kindly donated by Dr. M. Sanguinetti (University of Utah, Salt Lake City, UT, USA) and was subcloned into a pRc-CMV vector. A *KCNE1*-D85N variant was constructed using a Quik Change II XL Site-Directed Mutagenesis Kit, according to the manufacturer's instructions (Stratagene, La Jolla, California, USA). A *KCNH2* mutation (E58K) was constructed by overlap-extension PCR. Nucleotide sequence analysis was performed on each variant construct before the expression study to confirm their sequences.

2.3. Cell transfection

CHO cells were maintained at 37 °C in Dulbecco's modified Eagle medium and Ham's F12 nutritional mixture (Gibco-BRL, Rockville, Maryland, USA) containing 10% fetal bovine serum supplemented with 1% penicillin and 1% streptomycin. Wild-type (WT) and/or variant *KCNH2*, and WT and/or variant *KCNE1* clones were transiently expressed in CHO cells by using the Lipofectamine method according to the manufacturer's instructions (Invitrogen, Carlsbad, California, USA).

To identify the cells that were positive for *KCNH2* expression, CHO cells were co-transfected with 0.5–1 μg of the pRc-CMV/*KCNH2* vector and 0.5 μg of a pEGFP-N1/CMV vector. About 48–72 h after transfection, green fluorescent protein (GFP) positive cells and anti-CD8 antibody-coated bead (Dynabeads CD8; Dynal Biotech, Oslo, Norway) decorated cells were used for the patch-clamp study.

2.4. Electrophysiological assays

Whole-cell configuration of the patch-clamp technique was employed to record membrane currents at 37 °C with an EPC-8 patch-clamp amplifier (HEKA, Lambrecht, Germany). Pipette resistance ranged from 2.5 to 4 MΩ when filled with pipette solutions, as described in the following text. The series resistance was electronically compensated for at 70–85%. The extracellular solution contained (mmol/l): 140 NaCl, 0.33 NaH_2PO_4, 5.4 KCl, 1.8 $CaCl_2$, 0.5 $MgCl_2$, 5.5 glucose, and 5 HEPES and the pH was adjusted to 7.4 with NaOH. The internal (pipette) solution contained (mmol/l): 70 potassium aspartate, 70 KOH, 40 KCl, 10 KH_2PO_4, 1 Mg_2SO_4, 3 Na_2-ATP, 0.1 Li_2-GTP, 5 EGTA, and 5 HEPES and the pH was adjusted to 7.2 with KOH.

KCNH2/KCNE1-encoded currents were elicited by depolarizing pulses from a holding potential of −80 mV to test potentials between −60 and +50 mV (with a 10-mV step increment), and then repolarized to −60 mV to measure tail currents. Current densities (pA/pF) were calculated for each cell studied by normalizing peak tail current amplitude to cell capacitance (Cm). The Cm was calculated by fitting a single exponential function to the decay phase of the transient capacitive current in response to ±5 mV voltage steps (20 ms) from a holding potential of −50 mV. The liquid junction potential between the test solution and the pipette solution was measured as approximately −10 mV and was corrected. Data were collected and analyzed using Patch master and Igor Pro (WaveMetrics, Lake Oswego, Oregon, USA).

2.5. Data analyses

The voltage-dependence of current activation was determined by fitting the normalized tail current (I_{tail}) vs. test potential (Vt) to

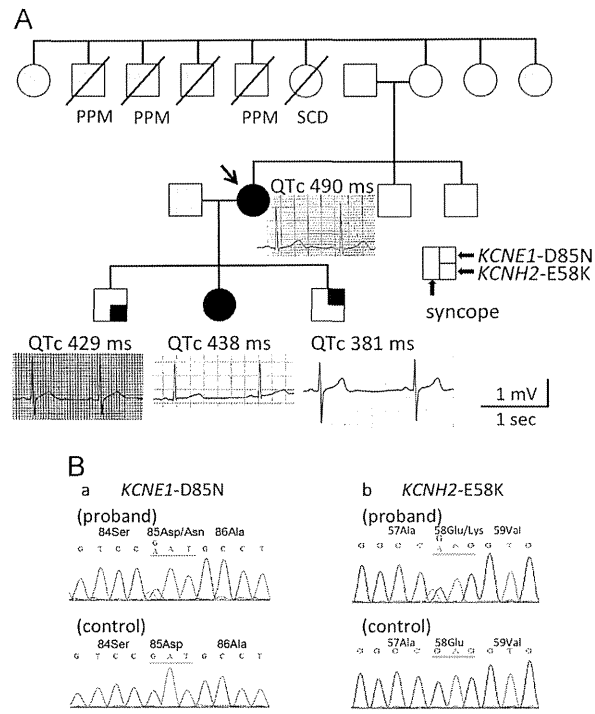

Fig. 1. Clinical Characteristics. A: Pedigree structures as well as phenotypic and genotypic information and electrocardiogram (V5) data for family members of the proband. Males and females are represented as squares and circles, respectively. Genotypes are shown on the right side of the symbols, and the presence of variants is indicated as shown in the inset. Phenotypes are shown in the left half of symbols. Filled symbols indicate symptomatic cases. Individuals with uncertain genotype and phenotype are indicated by a gray color. Deceased family members are indicated by symbols with slashes. PPM, post pacemaker implantation; SCD, sudden cardiac death. B: (a) The DNA sequence of D85N *KCNE1*; part of the nucleotide sequence of the *KCNE1* showing a G to A transition at codon 253 leading to an amino acid substitution of aspartic acid for asparagine at position 85. (b) The DNA sequence of E58K *KCNH2*; part of the nucleotide sequence of the *KCNH2* showing a G to A transition at codon 172 leading to an amino acid substitution of glutamine for lysine at position 58.

Boltzmann's function:

$I_{tail} = 1/(1+\exp[(V_{0.5}-Vt)/k])$,

where $V_{0.5}$ is the voltage at which the current is half-activated and k is the slope factor. Time constants for deactivation (τ_{fast} and τ_{slow}) were obtained by fitting a two-exponential function to the time course of the deactivating tail currents. All data were expressed as the mean ± standard error. Statistical comparisons were made using analysis of variance, followed by a t test, and the differences were considered significant at a value of $P < 0.05$.

3. Results

3.1. Clinical features

Among our 355 probands with mutations in *KCNQ1*, *KCNH2*, or *SCN5A*, 206 probands (58.0%) suffered cardiac events such as ventricular arrhythmia or syncope. The average QTc interval of 355 probands was 492.4 ± 55.7 ms. Fourteen probands (3.9%) carried a heterologous *KCNE1*-D85N polymorphism. Coexisting mutations were identified in either *KCNQ1* or *KCNH2* carriers. Ten mutations were missense, and the remaining 4 were complex deletion/insertion mutations in *KCNH2*. The average age of these subjects was 28 ± 18 years and females were the dominant gender (n=10, 71.4%). Eleven compound probands carrying *KCNE1*-D85N were symptomatic (78.5%), while 195 probands without *KCNE1*-D85N were symptomatic (57.1%, P=0.17). The average QTc interval of the probands with *KCNE1*-D85N was a little longer (503.6 ± 92.7 ms) than that of probands without *KCNE1*-D85N (491.8 ± 53.2 ms, P=0.64). In 7 of 14 probands, we failed to conduct genetic tests in their family members. In the remaining 7 families, we found a family in which both genetic variants were found in multiple family members (Fig. 1A). The proband (indicated by arrow in Fig. 1A) was a 51-year-old woman who was admitted to the hospital because of palpitations and repeated syncope. She experienced her first syncope at the age of 45. The standard 12-lead electrocardiogram (ECG) showed a prolonged QT interval (QT/QTc, 478/490 ms; HR, 63 bpm), notched T waves in leads II, III, and aV_F, and premature ventricular contraction. Blood and serological tests showed normal results. The echocardiogram, myocardial perfusion scintigraphy, and coronary angiography with/without acetylcholine test were all normal. Although ventricular fibrillation was not inducible on electrophysiological study, TdP with syncope was detected on the ECG monitor while she was talking to her doctor. Because she showed a marked sinus bradycardia (~40 bpm) during the day, a pacemaker was implanted and β-blocker therapy was started. Three uncles on her maternal side underwent pacemaker implantation and an aunt died suddenly before she reached 40-years-old (Fig. 1A).

The proband had 3 children (Fig. 1A), and her 2 sons were free of symptoms with normal QTc intervals (QTc, 429 ms and 381 ms, respectively). In contrast, her daughter experienced syncope several times since she was 13 years old. When the daughter was 22 years old, head-up tilt, exercise stress, and isoproterenol challenge tests were performed to examine the cause of syncope and she was suspected to have neurally mediated syncope. However, she repeated syncope while micturition at the age of 27 and she consequently underwent Holter monitoring. Because the ECG monitor demonstrated QT prolongation, she underwent an epinephrine challenge test. Intravenous administration of epinephrine (0.1 μg kg^{-1} plus 0.1 μg kg^{-1} min^{-1}) prolonged the QT interval (QTc, 438 to 658 ms) and she was diagnosed with LQTS.

3.2. Genetic analysis

DNA sequencing of the proband confirmed a G to A transition leading to amino acid substitution of aspartic acid for asparagine at position 85 (D85N) located within the C-terminal region of *KCNE1* (Fig. 1B-a) and a G to A transition leading to amino acid substitution of glutamic acid for lysine at position 58 (E58K) in the N-terminus of *KCNH2* (Fig. 1B-b). We identified 2 heterozygous variants, *KCNH2*-E58K and *KCNE1*-D85N, in the proband and her daughter. The proband's elder son had *KCNH2*-E58K and the younger son had *KCNE1*-D85N, respectively. In this family, therefore, a genetic double hit appeared to largely modify the clinical phenotypes (Fig. 1A).

3.3. Biophysical assays

To examine the phenotype–genotype correlation, we first examined how the *KCNH2*-E58K mutation affected I_{Kr} currents when reconstituted in CHO cells. Fig. 2 depicts 3 sets of typical current traces recorded from cells transfected with *KCNH2*-WT (A, 1 μg), *KCNH2*-WT/E58K (B, 0.5 μg each), and *KCNH2*-E58K (C, 1 μg). Cells transfected with *KCNH2*-WT displayed inwardly

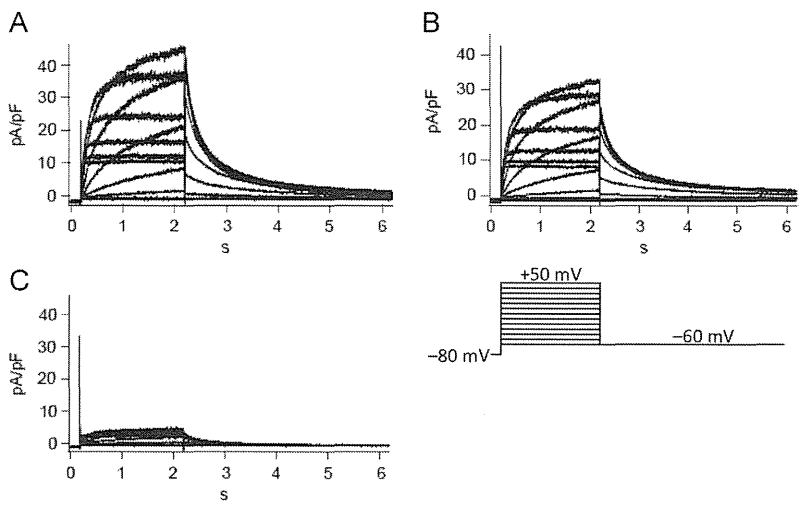

Fig. 2. Functional expression analysis of *KCNH2* in Chinese hamster ovary cells. Representative current traces of KCNH2 co-expression with the WT and/or E58K. (A) *KCNH2*-WT (1 μg). (B) *KCNH2*-WT/E58K (0.5 μg of each). (C) *KCNH2*-E58K (1 μg).